Published in final edited form as:
Annu Rev Phys Chem. 2010 March ; 61: 461–485. doi:10.1146/annurev.physchem.012809.103436.

Fluctuations in Biological and Bioinspired Electron-Transfer Reactions

Spiros S. Skourtis[1], **David H. Waldeck**[2], and **David N. Beratan**[3]

[1]Department of Physics, University of Cyprus, Nicosia 1678, Cyprus; skourtis@ucy.ac.cy

[2]Department of Chemistry, University of Pittsburgh, Pittsburgh, Pennsylvania 15260; dave@pitt.edu

[3]Departments of Chemistry and Biochemistry, Duke University, Durham, North Carolina 27708; david.beratan@duke.edu

Abstract

Central to theories of electron transfer (ET) is the idea that nuclear motion generates a transition state that enables electron flow to proceed, but nuclear motion also induces fluctuations in the donor-acceptor (DA) electronic coupling that is the rate-limiting parameter for nonadiabatic ET. The interplay between the DA energy gap and DA coupling fluctuations is particularly noteworthy in biological ET, where flexible protein and mobile water bridges take center stage. Here, we discuss the critical timescales at play for ET reactions in fluctuating media, highlighting issues of the Condon approximation, average medium versus fluctuation-controlled electron tunneling, gated and solvent relaxation controlled electron transfer, and the influence of inelastic tunneling on electronic coupling pathway interferences. Taken together, one may use this framework to establish principles to describe how macromolecular structure and structural fluctuations influence ET reactions. This framework deepens our understanding of ET chemistry in fluctuating media. Moreover, it provides a unifying perspective for biophysical charge-transfer processes and helps to frame new questions associated with energy harvesting and transduction in fluctuating media.

Keywords

coupling fluctuations; tunneling pathways; inelastic tunneling; pathway coherence; solvent dynamical effects; water-mediated tunneling

1. INTRODUCTION

Is the reactivity of biomolecules dictated by their average molecular structure, by routine thermal excursions from the average, or by rare large-scale conformational changes? Addressing these questions is central to establishing a description of bioenergetics at the molecular scale. Here, we address these and closely related issues in the framework of biological and bioinspired electron transfer (ET). We review how a new generation of theory and experiments is unveiling the role played by protein and solution structure, fluctuations, and relaxation in ET kinetics and mechanisms.

DISCLOSURE STATEMENT

The authors are not aware of any affiliations, memberships, funding, or financial holdings that might be perceived as affecting the objectivity of this review.

Early formulations of nonadiabatic ET reactions were based on Fermi's golden rule and emphasized the probability of encountering configurations with quasi-degenerate donor and acceptor states (through the Franck-Condon factor), and the propensity for electron tunneling in these configurations (through the tunneling matrix element). Recent studies have focused on how structural fluctuations [those generating donor-acceptor (DA) degeneracy and others] may influence the transfer rate, revealing a richness of mechanistic behavior.

The familiar Fermi's golden-rule ET rate constant is $k_{ET}=\frac{2\pi}{\hbar}T_{DA}^2(F.C.)$, where T_{DA} is the DA electronic coupling interaction and ($F.C.$) is the Franck-Condon factor (1–7). The description of ET in terms of a single rate constant suggests that the ET kinetics is single exponential and it is appropriate if $1/k_{ET}$ is slow compared with timescales of fluctuations that may modulate the reaction rate. Such fluctuations could include conformational interconversions and solvent relaxation. These molecular fluctuations may affect both the DA energy gap and the DA tunneling matrix element, and the fluctuations may lead to regimes that require modification of the golden-rule rate constant, even in the limit of single exponential kinetics.

2. COUPLING FLUCTUATION EFFECTS IN ELECTRON TRANSFER

In the following, we discuss generalizations of the nonadiabatic ET rate expression when fluctuations of the molecular structure and of the solvent modulate T_{DA} with a fluctuation timescale that is fast compared with $1/k_{ET}$. When the coupling fluctuations are slow on the timescale of nuclear motion through the crossing region of the donor and acceptor potential surfaces (validating the Condon approximation), T_{DA}^2 in the nonadiabatic rate expression should be replaced by its thermal average $\left\langle T_{DA}^2 \right\rangle$. If the coupling fluctuations are fast on the timescale of nuclear motion through the crossing region, the tunneling electron may exchange energy with the nuclear degrees of freedom of the bridge, enabling inelastic tunneling. This effect has a well-understood influence on the Franck-Condon factor and can also change T_{DA} significantly, as inelastic markers left on tunneling pathways change the overall amplitude for tunneling (vide infra).

We now present a framework for exploring how bridge fluctuations influence ET kinetics. We use a time-dependent version of Fermi's golden rule with a semiclassical approximation to explore the relevant timescales, both in general and for some specific systems. It is helpful to express the nonadiabatic ET rate constant as the Fourier transform of time-dependent correlation functions (see 8,9). We consider an ET system described by the Hamiltonian $\hat{H} = \hat{H}^D + \hat{H}^A + \hat{H}^B + \hat{V}$, where $\hat{H}^D$ and $\hat{H}^A$ are electronic-vibrational (vibronic) Hamiltonians for the donor (D) and acceptor (A) diabatic potential surfaces (Figure 1), $\hat{H}^B$ is the vibronic bridge Hamiltonian, and $\hat{V}$ couples donor (acceptor) and bridge electronic states. In particular, $\widehat{H}^D=U_D^{\min}|D\left\langle D|+\widehat{H}^{D(vi)}\right.$ and $\widehat{H}^A=U_A^{\min}|A\left\rangle\right\langle A|+\widehat{H}^{A(vi)}$, where $\hat{H}^{D(vi)}$ and $\hat{H}^{A(vi)}$ are the vibrational Hamiltonians for the U_D and U_A harmonic diabatic surfaces (Figure 1), and $\hat{H}^B = \hat{H}^{B(el)} + \hat{H}^{B(vi)} + \hat{H}^{B(e-v)}$, where $\hat{H}^{B(el)}$ and $\hat{H}^{B(vi)}$ are the electronic and vibrational bridge Hamiltonians, respectively. $\hat{H}^{B(e-v)}$ describes the bridge electronic-vibrational interactions. In this model, the nonadiabatic ET rate constant is

$$k_{ET}(\omega_{DA})=\frac{1}{\hbar^2}\int_{-\infty}^{+\infty}dt e^{i\omega_{DA}t}C_{T_{DA}}(t)C_{FC}(t), \quad (1)$$

where $\omega_{DA}=(U_D^{\min}-U_A^{\min})/\hbar$ is the frequency corresponding to the energy gap (Figure 1), $C_{FC}(t)$ is the time-dependent Franck-Condon factor,

$$C_{FC}(t)=\left\langle e^{i\widehat{H}^{D(vi)}t/\hbar}e^{-i\widehat{H}^{A(vi)}t/\hbar}\right\rangle_D, \tag{2}$$

and

$$C_{T_{DA}}(t)=\left\langle \widehat{T}_{DA}(t)\widehat{T}_{DA}(0)\right\rangle_B=\left\langle e^{i\widehat{H}^{B(vi)}t/\hbar}\widehat{T}_{DA}(0)e^{-i\widehat{H}^{B(vi)}t/\hbar}\widehat{T}_{DA}(0)\right\rangle_B \tag{3}$$

is the correlation function of the vibronic DA electronic coupling (tunneling matrix element). $\langle\ldots\rangle_D$ and $\langle\ldots\rangle_B$ denote thermal averages over the $\hat{H}^{D(vi)}$ and $\hat{H}^{B(vi)}$ vibrational eigenstates, respectively. The vibronic tunneling matrix element to second order in $\hat{V}$ is

$$\widehat{T}_{DA}(0)=\widehat{V}(E_{tun}-\widehat{H}^B)^{-1}\widehat{V}, \tag{4}$$

where E_{tun} is the total electronic-vibrational energy of the system when the electron is in the initial donor electronic state (10–12).

In the high-temperature (classical) limit for the donor and acceptor vibrational degrees of freedom,

$$C_{FC}(t)\approx e^{-i\lambda t/\hbar}e^{-t^2/2\tau_{FC}^2}, \tag{5}$$

where λ is the reorganization energy (Figure 1), and $\tau_{FC}=\hbar/\sqrt{2\lambda k_B T}$ is often called the Franck-Condon time (5,7). The Franck-Condon time can be interpreted as the characteristic time for the system to move out of the DA diabatic surface crossing region (Figure 1) due to thermal fluctuations of the DA energy gap, i.e.,

$$\tau_{FC}=\hbar/\sigma_{\Delta U,}\ \text{where}\ \sigma_{\Delta U}^2=\left\langle(\widehat{H}^{A(vi)}-\widehat{H}^{D(vi)})^2\right\rangle-\left\langle(\widehat{H}^{A(vi)}-\widehat{H}^{D(vi)})\right\rangle^2=2\lambda k_B T.$$

In the classical limit for the bridge vibrational degrees of freedom, the electronic coupling depends parametrically on the atom trajectories, and the correlation function is

$$C_{T_{DA}}(t)=\langle T_{DA}(t)T_{DA}(0)\rangle, \tag{6}$$

where $\langle\ldots.\rangle$ denotes a classical thermal average. In practice, $T_{DA}(t)$ is computed along classical molecular dynamics (MD) trajectories, i.e., $T_{DA}(t)=T_{DA}[\{\vec{r}_1(t),\ldots.\vec{r}_N(t)\}]$, where $\vec{r}_i(t)$ is the position of atom i, and $\langle..\rangle$ is the time (trajectory) average. A perturbative expression for $T_{DA}(t)$ in a nonorthogonal donor, acceptor, and bridge (i_B, j_B) basis is

$$T_{DA}(t)=\sum_{i_B}\sum_{j_B}(E_{tun}^{(el)}S_{D,i_B}-V_{D,i_B})G_{i_B,j_B}(E_{tun}^{(el)})(E_{tun}^{(el)}S_{j_B,A}-V_{j_B,A}), \tag{7}$$

where $G_{i_B,j_B}(E_{tun}^{(el)})=\{(E_{tun}^{(el)}\tilde{S}^{B(el)}-\tilde{H}^{B(el)})^{-1}\}_{i_B,j_B}$ is the matrix element of the electronic bridge Green's function; S_{ij} and V_{ij} are donor- (acceptor-) to-bridge overlap and electronic

Hamiltonian matrix elements, respectively; and $\tilde{S}^{B(el)}$ and $\tilde{H}^{B(el)}$ are bridge overlap and electronic Hamiltonian matrices (13). $E_{tun}^{(el)}$ is the tunneling energy of the electron. All quantities on the right-hand side of Equation 7, including the tunneling energy, should be evaluated at time t (14,15).

$T_{DA}(t)$ is routinely computed using a variety of approaches, including Green's function and energy-splitting analysis (11), generalized Mulliken-Hush analysis (16), and tunneling current methods (17). The timescale of $T_{DA}(t)$ fluctuations is characterized by the coherence time (τ_{coh}) (8,18,19). τ_{coh} is the decay time of the $C_{T_{DA}}(t)$ correlation function; it measures how rapidly fluctuations of the electronic coupling randomize $T_{DA}(t)$ values, e.g.,

$$C_{T_{DA}}(t) \approx \sigma_{T_{DA}}^2 e^{-t^2/2\tau_{coh}^2 + \langle T_{DA}\rangle^2}, \tag{8}$$

where $\sigma_{T_{DA}} = \sqrt{\langle T_{DA}^2\rangle - \langle T_{DA}\rangle^2}$. For small times compared with τ_{coh}, $C_{T_{DA}}(t)$ approaches the value $\langle T_{DA}^2\rangle$; for long times compared with τ_{coh}, $C_{T_{DA}}(t)$ approaches $\langle T_{DA}\rangle^2$. The strength of $T_{DA}(t)$ fluctuations is characterized by

$$R_{coh} = \frac{\langle T_{DA}\rangle^2}{\langle T_{DA}^2\rangle} = \frac{1}{1+(\sigma_{T_{DA}}^2/\langle T_{DA}\rangle^2)}, \tag{9}$$

which is known as the coherence parameter (20). When coupling fluctuations are large compared with the average coupling $(\sigma_{T_{DA}}^2 \gg \langle T_{DA}\rangle^2)$, the coherence parameter is small, $R_{coh} \ll 1$, and for small fluctuations $(\sigma_{T_{DA}}^2 \ll \langle T_{DA}\rangle^2)$, $R_{coh} \approx 1$.

The parameters R_{coh}, τ_{coh}, and τ_{FC} are useful to describe distinct nonadiabatic ET rate regimes (see 8,18,19,21). We focus next on single exponential ET kinetics. In this regime, we have $\tau_{FC}, \tau_{coh} \ll 1/k_{ET}$ [if any of the timescales is longer than the ET time, the kinetics may be multi-exponential or gated (22,23)].

3. THE SLOW COUPLING–FLUCTUATION REGIME ($\tau_{coh} > \tau_{FC}$)

In this regime, $T_{DA}(t)$ does not fluctuate while the donor and acceptor electronic states are in resonance. As a result, each DA energy crossing event is subject to an effectively constant coupling, equal to the value of $T_{DA}(t)$ at the time of the crossing (i.e., the Franck-Condon approximation is valid). In Equation 1, we can thus replace $C_{T_{DA}}(t)$ by $C_{T_{DA}}(0) = \langle T_{DA}^2\rangle$, and the rate is proportional to the product of $\langle T_{DA}^2\rangle$ and the Franck-Condon weighted density of states, $\rho_{FC} = (4\pi\lambda k_B T)^{-1/2} e^{-([U_D^{\min} - U_A^{\min}] - \lambda)^2/4\lambda k_B T}$ [assuming the classical high-temperature expression for $C_{FC}(t)$ in Equation 5]. Here, one finds two limits: the weak T_{DA} fluctuation regime ($R_{coh} \approx 1$) and the strong T_{DA} fluctuation regime ($R_{coh} \ll 1$).

In the limit of weak T_{DA} fluctuations, bridge fluctuations do not change T_{DA} significantly. Hence, $\langle T_{DA}^2\rangle \approx \langle T_{DA}\rangle^2$, and the rate is

$$k_{ET} = \frac{2\pi}{\hbar}\langle T_{DA}\rangle^2 \rho_{FC}. \tag{10}$$

This limit applies to a broad range of ET model systems with the donor and acceptor linked by rigid bridges. Paddon-Row and coworkers (24,25), Miller and coworkers (26), Newton and coworkers (27), and others (6) have investigated ET kinetics in chemical systems with rigid organic bridges (Figure 2). Through the use of beautifully designed molecular structures and many different kinetic probes, investigators have shown that nonadiabatic ET in such systems proceeds via bridge-mediated electron or hole tunneling. Furthermore, the tunneling propensity is described by T_{DA} values that correspond to equilibrium bridge structures (see 4,27,28 for reviews of these studies). In these systems, thermal fluctuations of the bridge structure do not cause significant changes in T_{DA} (i.e., $\sigma^2_{T_{DA}} \ll \langle T_{DA}\rangle^2$).

In the case of near-zero T_{DA} values for the equilibrium bridge structure, T_{DA} fluctuations can induce large changes in T_{DA} compared with the average, i.e., $\sigma^2_{T_{DA}} \gg \langle T_{DA}\rangle^2 (R_{coh} \ll 1)$. In this regime, bridge structural fluctuations enhance the coupling and determine the observed ET rate constant,

$$k_{ET} = \frac{2\pi}{\hbar}\left\langle T^2_{DA}\right\rangle \rho_{FC}. \tag{11}$$

Here, one expects that the ET rate can increase with increasing temperature because the system accesses bridge conformations with larger couplings (9,23). Whereas the regime of large T_{DA} fluctuations has wide applicability in long-distance biological ET, the studies of Zimmt and Waldeck show that the fluctuation-dominated regime can also be relevant to small chemical ET systems (vide infra). Using synthetic donor-bridge-acceptor structures where a cleft (i.e., a C-clamp) forms between donor and acceptor, they (30,31) showed that ET occurs by electron (hole) tunneling through a solvent in the cleft (Figure 2). Their studies reveal that the electronic coupling could not be described using a static perspective but must be described by a temperature-dependent dynamical perspective (32). By design, these C-clamp structures have a zero average electronic coupling because of symmetry, so configurational fluctuations (donor-solvent-acceptor) are essential for the enhancement of the DA coupling; such systems provide an important testing ground for understanding the fluctuation-controlled transfer regime (33). A recent extension of this idea to water-soluble cleft molecules (see Figure 3) promises to provide a way to investigate electron tunneling through water molecules.

Expanding $C_{T_{DA}}(t)$ to second order in time, it is possible to write the ET rate in powers of (τ_{FC}/τ_{coh}): $C_{T_{DA}}(t) = C_{T_{DA}}(0) + \dot{C}_{T_{DA}}(0)t + \ddot{C}_{T_{DA}}(0)t^2/2$. With $C_{FC}(t) \propto e^{-i\lambda t/\hbar} e^{-t^2/2\tau^2_{FC}}$ and $C_{T_{DA}}(t) \approx \sigma^2_{T_{DA}} e^{-t^2/2\tau^2_{coh}} + \langle T_{DA}\rangle^2$, one finds

$$k_{ET} = \left\langle T^2_{DA}\right\rangle \rho_{FC}[\,1+\delta k], \tag{12}$$

where δk is the non-Condon correction to the rate equation of the slow fluctuation regime (Equation 11), to lowest order (second order) in (τ_{FC}/τ_{coh}) (8). Here, δk depends on R_{coh} and $U^{\min}_D - U^{\min}_A$ [in addition to $(\tau_{FC}/\tau_{coh})^2$], and it can be computed using MD simulations.

Numerous studies of ET reactions have examined the fluctuation dependence of the DA coupling (14,15,21,28,33–40), with the aim of identifying bridge conformations that enhance this coupling. Three studies (18,19,21) characterize known ET reactions in terms of R_{coh}, τ_{coh}, and δk (using MD simulations and semiempirical electronic structure analysis) to understand how these parameters relate to bridge structure and dynamics. Comparison of the results (18,19,21) is instructive because Reference 18 explores short-range solvent-mediated

ET in the C-clamped molecules above, Reference [19] explores long-distance ET in the protein azurin, and Reference [21] studies ET in the photosynthetic reaction $BPh^- \rightarrow Q_A$ in the bacterial photosynthetic reaction center. In these three cases, the computed non-Condon correction values are similar ($\delta k \leq 1\%$), which means that the ET rates for all these systems are well described using Equation 11. The coherence parameters vary from $R_{coh} \leq 0.1$ for References [18] and [19] (strong T_{DA} fluctuations) to 0.4 for Reference [21] (moderate T_{DA} fluctuations). Surprisingly, the τ_{coh} values are similar for all ET reactions in these studies (τ_{coh} is a few tens to 100 fs). In all cases, the tunneling matrix element fluctuations are slow ($\tau_{coh} > \tau_{FC}$), and this observation may be understood using simple arguments. For ET reactions with $\lambda \approx 1$ eV, the room-temperature Franck-Condon time is expected to be very short, $\tau_{FC}=\hbar/\sqrt{2\lambda k_B T}\sim$fs [for azurin $\tau_{FC} \approx 3-4$ fs, as computed using MD simulations (41), and for the C-clamp molecules (Figure 2), a range of τ_{FC} values that depend on the solvent are possible and have magnitudes of a few femtoseconds (18)]. Constrained MD simulations for azurin (19) show that the fastest bridge motions that determine τ_{coh} are largely valence angle vibrations with periods of a few tens of femtoseconds, much longer than the typical τ_{FC} times discussed above. Such vibrations have similar periods for a wide variety of chemical bridges, suggesting that the slow fluctuation regime is general for ET tunneling reactions at room temperature in polar media, with ~1-eV reorganization energies, normal (unstrained) chemical bridges, and Gibbs free energy gaps that do not place the ET reaction in the highly activated regime. Deviations from the regime of slow matrix element fluctuations could arise for systems with longer Franck-Condon times (see [42],43 for deviations from the formula $\tau_{FC}=\hbar/\sqrt{2\lambda k_B T}$) and are more likely for low-bridge-gap tunneling systems, where the tunneling matrix element is sensitive to bridge deformations (11,19,44).

3.1. The Characteristic Length r_{crit}

It is interesting to examine why short-distance ($R_{DA} \sim 7$ Å) solvent-mediated ET in the C-clamp molecules (18) shows equally strong tunneling matrix element fluctuations as are found in long-distance ($R_{DA} \sim 17$–24 Å) protein-mediated ET in azurin (19) ($R_{coh} \leq 0.1$ in both cases). Recent studies (45) suggest that there is a critical (medium-dependent) distance beyond which DA coupling fluctuations dominate the electron tunneling. Indeed, Reference 45 poses a statistical question regarding coupling: Is there a distance r_{crit} that characterizes, on average, a transition between $\langle T_{DA}\rangle^2$ and $\sigma^2_{T_{DA}}$ dominated kinetics? An answer to this question emerges from an electronic coupling analysis for MD sampled geometries of Ru-modified heme and blue-copper proteins (46), as well as for water-mediated self-exchange between cytochrome b_5 molecules. (47) For the protein-mediated tunneling systems, the transition between the $\langle T_{DA}\rangle^2$-dominated regime and the $\sigma^2_{T_{DA}}$-dominated regime occurs at distances of ~6–7 Å, about the size of an amino acid residue (see Figure 4*a*). For the water-mediated self-exchange reaction, the transition to a fluctuation-dominated coupling regime occurs at distances about the size of a water molecule, ~2–3 Å (Figure 4*a*). Importantly, these critical distances for protein and water tunneling media coincide with the computed mechanical (κ_{ij}) and electron-tunneling (χ_{ij}) spatial correlation functions (45):

$$\kappa_{ij}=\frac{\left\langle (\vec{r}_i-\left\langle \vec{r}_i\right\rangle)(\vec{r}_j-\left\langle \vec{r}_j\right\rangle)\right\rangle}{\sqrt{\left\langle (\vec{r}_i-\left\langle \vec{r}_i\right\rangle)^2\right\rangle\left\langle (\vec{r}_j-\left\langle \vec{r}_j\right\rangle)^2\right\rangle}},\quad \chi_{ij}=\frac{\left\langle (G_{ii}^2-\left\langle G_{ii}^2\right\rangle)(G_{ij}^2-\left\langle G_{ij}^2\right\rangle)\right\rangle}{\sqrt{\left\langle (G_{ii}^2-\left\langle G_{ii}^2\right\rangle)^2\right\rangle\left\langle (G_{ij}^2-\left\langle G_{ij}^2\right\rangle)^2\right\rangle}}. \quad (13)$$

Here, $\vec{r}_i$ represent bridging atom positions, and G_{ij} is the bridge electronic Green's function between two-center bond orbitals *i* and *j* (Equation 7). κ_{ij} describes the loss of correlation

among atomic motions that arises from thermal fluctuations of the bridge structure, and χ_{ij} describes the loss of correlation among electron-tunneling propagations through the bridge that involves different tunneling distances. The loss of tunneling correlation is also a function of the bridge structural fluctuations. For both water and protein media, the κ_{ij} and χ_{ij} decay (correlation) lengths coincide with r_{crit} for which, on average, $\langle T_{DA}\rangle^2=\sigma^2_{T_{DA}}$. Thus, the onset of a fluctuation-dominated regime is related to the loss of mechanical and tunneling-propagation correlation in the bridge. For water-mediated tunneling, mechanical and tunneling correlation is lost, on average, for distances greater than the size of a water molecule, whereas for proteins, this distance is larger on average (45). The water results suggest that, for solvent-mediated ET in general, the fluctuation-dominated regime will occur at distances greater than the size of the solvent molecules. This analysis explains the results that find ET in C-clamp molecules (R_{DA} ~ 7 Å) and in azurin (R_{DA} ~ 17–24 Å) to be fluctuation dominated (18, 19). Even though the tunneling distances are different in the two systems, they are each larger than the critical distance for the respective tunneling media. It would be interesting to repeat the above analysis for the $BPh^- \rightarrow Q_A$ ET reaction, where R_{coh} = 0.4 (21).

In Gray & Winkler's (46) tunneling-limited Ru-modified protein ET experiments, all derivatives with anomalously slow rates for their DA distance (in the heme proteins myoglobin, cytochrome *c*, and cytochrome b_{562}) are in the weak fluctuation regime $(\langle T_{DA}\rangle^2<\sigma^2_{T_{DA}})$ and have only a few coupling pathways, which are axial to the heme donor. Protein derivatives with fast and average rates (for their distance) fall in the strong fluctuation regime $(\langle T_{DA}\rangle^2>\sigma^2_{T_{DA}})$ and have tunneling matrix elements that are determined by interactions among many alternative pathway structures, rather than by a few dominant paths (48). The above observations suggest a useful hierarchy for categorizing protein structural effects on ET. At a first coarse level, rates drop rapidly as a function of distance because of the underlying tunneling mechanism. At a second level, rates through β-strands are more rapid for their distance than for α-helices at the same distance as a consequence of tunneling pathway length effects (49). At a third level, edge-coupled hemes and chlorophylls tend to sample many interfering pathways and will have fluctuation-dominated and multipathway-mediated tunneling. As we discuss below, fluctuation-dominated coupling need not wash out the influence of the protein's fold on the ET rate; rather, it seems likely that it may remove the possibility of a single weak link causing dramatic slowing (for a given distance) (50).

3.2. Fluctuations and Structure

A natural question that arises from an analysis of how fluctuations impact ET kinetics is whether fluctuations wash out the influence of medium structure on the ET rates. This question has been addressed within the database of protein-mediated ET (in the case of Ru proteins) and water-mediated ET (for cytochrome b_5 self-exchange) (45). If tunneling medium fluctuations wash out structural features, the tunneling medium could be described by an effective structureless tunneling barrier. To address this key issue, which has deep connections to the role of evolution in determining tunneling pathway structure (48,51–54), we computed the metric (45)

$$S[\langle T^2_{DA}\rangle]_{R_{DA}}=\frac{\sqrt{var[\langle T^2_{DA}\rangle]_{R_{DA}}}}{avg[\langle T^2_{DA}\rangle]_{R_{DA}}}, \quad (14)$$

where the variance (*var*) and the average (*avg*) are computed for all distinct ET species with the same transfer distance. A value of $S_{R_{DA}} \ll 1$ at a given R_{DA} means that an average barrier

model that reproduces $avg[\langle T_{DA}^2 \rangle]_{R_{DA}}$ gives, to a good approximation, $\langle T_{DA}^2 \rangle$ for all ET species at R_{DA}. A value of $S_{R_{DA}} \geq 1$ means that the $\langle T_{DA}^2 \rangle$ for any single ET species is not representative of the $\langle T_{DA}^2 \rangle$ for the other ET species at that distance (Figure 5).

We find that $S_{R_{DA}}$ is of order unity for all transfer distances (Figure 4*b*), indicating that the influence of structural differences between proteins on the mean-squared ET couplings is large. Even at large R_{DA}, where $\sigma_{T_{DA}}^2$ dominates, the diversity of values at any distance is not washed out by structural fluctuations. Thus, the protein structure defines the tunneling rates, even when fluctuations dominate the ensemble of coupling values. This seems to be the case even for water-mediated interprotein ET (45).

The fluctuation analysis described here has been used mostly to study small-molecule and protein ET, although there is a growing body of related work on nucleic acids (see 55, and references therein). It will be interesting to use the parameters defined above to characterize fluctuations and structural disorder in DNA ET reactions. The DNA ET mechanism may vary from tunneling to thermally activated hopping, so that a simple tunneling element analysis may not describe the kinetics (44,56,57). Moreover, the folded structure of DNA does not show the wide variability found in proteins, so it may be interesting to study the dependency of R_{coh} and $S_{R_{DA}}$ on sequence, rather than on distance. The coherence parameter approach was recently applied to DNA charge transfer (58,59).

MOLECULAR C-CLAMPS: INTERPOSING A WATER MOLECULE THAT MEDIATES TUNNELING BETWEEN DONOR AND ACCEPTOR

Modern synthetic tools allow the synthesis of tailored cleft or C-clamp structures, in which the dimensions of the C-clamp define the tunneling medium. The structure D-SSS-A (see Figure 3) has the dimensions and shape that will permit one water molecule to bridge between the donor and acceptor, but one DMSO molecule is too large to fit. The observed ET rate for D-SSS-A in water is much larger than that in DMSO. For the structure D-SRR-A, in which the dominant tunneling paths are through bonds, the ET rates are about the same in the two solvents (29).

WHAT ARE THE CHARACTERISTICS OF PROTEINS WITH LARGE VERSUS SMALL FLUCTUATIONS IN THE DONOR-ACCEPTOR TUNNELING INTERACTION, T_{DA}?

Proteins are dynamical objects: Their geometries fluctuate so the interactions that they mediate between redox cofactors that bind to them also fluctuate. Figure 5 illustrates the small versus large DA fluctuation regimes. In the small fluctuation regime, the width of the T_{DA} distributions for pairs of cofactors bound at different sites with the same DA separation distances (R_{DA}) is narrow compared to the differences in the $\langle T_{DA}^2 \rangle$ values. When fluctuations are large, the fluctuations may cause the differences in the mean-squared $\langle T_{DA}^2 \rangle$ values to become quite similar.

4. THE FAST COUPLING–FLUCTUATION REGIME ($\tau_{coh} \leq \tau_{FC}$)

In this regime, $T_{DA}(t)$ fluctuates while the donor and acceptor are resonant, so the Franck-Condon approximation may not be valid. In this limit, the rate equation is more complex than suggested by Equation 11 because there is no clear separation between the $C_{FC}(t)$ and

$C_{T_{DA}}(t)$ timescales in Equation 1. Theoretical studies of how matrix element fluctuations influence ET rates demonstrate the existence of various kinetic regimes (8, 23, 60–68). In the fast fluctuation limit ($\tau_{coh} < \tau_{FC}$) and for activationless (or nearly activationless) ET, the rate decreases with decreasing τ_{coh} because fluctuations take the system out of the activationless regime. For large activation free energies, the fluctuations can enhance the rate. In general, this rate enhancement is more pronounced in the inverted region because of inelastic transitions, and the overall effect is to reduce the drop in rate with increasing energy gap (and to change the rate's temperature dependence).

Inelastic tunneling introduces the exchange of energy between the tunneling electron and the bridge vibrations. If bridge vibrations are described quantum mechanically, the nonadiabatic rate expression is (8,12,65) $k_{ET} = \sum_i P_{\nu_i} \sum_f k_{ET}(\nu_i \rightarrow \nu_f)$, where

$$k_{ET}(\nu_i \rightarrow \nu_f) = (2\pi/\hbar)|\left\langle D;\nu_i|\widehat{T}|A;\nu_f\right\rangle|^2 \times \rho_{FC}(\nu_i \rightarrow \nu_f), \tag{15}$$

assuming thermal equilibration of the vibrational degrees of freedom prior to ET. k_{ET} is a thermally weighted sum of individual rates $k_{ET}(\nu_i \rightarrow \nu_f)$, each associated with a ν_i-to-ν_f transition induced by the exchange of energy with the tunneling electron (ν_i and ν_f are initial and final bridge vibrational states, respectively). The statistical weights, P_{ν_i}, are Boltzmann populations of initial ν_i states. $k_{ET}(\nu_i \rightarrow \nu_f)$ in Equation 15 contains a vibronic tunneling matrix element $\langle D; \nu_i|\hat{T}|A; \nu_f\rangle$ ($\hat{T}$ is given in Equation 4) and a thermally weighted Franck-Condon factor $\rho_{FC}(\nu_i \rightarrow \nu_f)$. If the vibrational degrees of freedom associated with the donor and acceptor diabatic surfaces (Figure 1) are treated classically,

$$\rho_{FC}(\nu_i \rightarrow \nu_f) = (4\pi\lambda k_B T)^{-1/2} \exp[-([U_D^{\min} + \varepsilon_{\nu_i} - (U_A^{\min} + \varepsilon_{\nu_f})] - \lambda)^2/4\lambda k_B T], \tag{16}$$

where ε_{ν_i} and ε_{ν_f} are the energies of bridge vibrational states ν_i and ν_f, and λ is the reorganization energy of the donor and acceptor diabatic surfaces (Figure 1). Equation 16 shows that the energy gap for elastic tunneling ($\varepsilon_{\nu_i} = \varepsilon_{\nu_f}$) is $U_D^{\min} - U_A^{\min}$, regardless of the initial (final) bridge vibrational state. For inelastic tunneling ($\varepsilon_{\nu_i} \neq \varepsilon_{\nu_f}$), the energy gap is shifted by an amount equal to the change in the bridge vibrational energy, given by $U_D^{\min} + \varepsilon_{\nu_i} - (U_A^{\min} + \varepsilon_{\nu_f}) = U_D^{\min} - U_A^{\min} + (\varepsilon_{\nu_i} - \varepsilon_{\nu_f})$, and it can have a strong effect on the ET rate. For an elastic ET reaction strongly in the inverted regime, the elastic ET rate is suppressed by the large activation energy; e.g., if $U_D^{\min} = U_A^{\min} + 2\lambda$ and $\lambda \gg k_B T$, then $E_{act} = (U_D^{\min} - U_A^{\min} - \lambda)^2/4\lambda = \lambda/4 \gg k_B T$. If a bridge vibration with frequency $\hbar\omega \approx \lambda$ can interact with the tunneling electron, however, then inelastic tunneling is possible because the electron can deposit energy equal to λ in any state ν_i of the oscillator, exciting it to state ν_f with $\varepsilon_{\nu_i} - \varepsilon_{\nu_f} = -\hbar\omega = -\lambda$. The corresponding rate $k_{ET}(\nu_i \rightarrow \nu_f)$ is activationless because its energy gap is reduced by λ, i.e., $E_{act} = ([U_D^{\min} + \varepsilon_{\nu_i} - (U_A^{\min} + \varepsilon_{\nu_f})] - \lambda)^2/4\lambda = 0$. Therefore, inelastic tunneling rates in the inverted region are enhanced, and the overall rate does not drop by the amount predicted for pure elastic tunneling. The effect is stronger for large bridges where the bridge vibrational spectrum is very dense (65). Enhanced ET rates in the inverted regime have been reported for small-molecule ET (69) and for biological ET (70), although it is not clear that the enhancement arises from inelastic tunneling.

We now explore how tunneling interactions, $\langle D; \nu_i|\hat{T}|A; \nu_f\rangle$ in Equation 4, change when the tunneling is inelastic. We consider a bridge with two parallel electronic pathways (bridge orbitals *B*1 and *B*2 both coupled to the *D* and *A* states; see Figure 6), where each bridge orbital

energy is modulated by a pathway-specific bridge vibrational mode (y_1 for $B1$ and y_2 for $B2$). Assuming linear electronic-vibrational coupling, we have, in Equation 4, $\hat{H}^B = \hat{H}^{B(el)} + \hat{H}^{B(vi)} + \hat{H}^{B(e-v)}$, where

$$\widehat{H}^{B(el)} = U_{B1}^{\min} |B1\rangle\langle B1| + U_{B2}^{\min} |B2\rangle\langle B2|, \tag{17}$$

$$\widehat{H}^{B(vi)} = \sum_n \hbar\omega_1 (n+1/2) |n(y_1)\rangle\langle n(y_1)| + \sum_m \hbar\omega_2 (m+1/2) |m(y_2)\rangle\langle m(y_2)|, \tag{18}$$

and

$$\widehat{H}^{B(e-v)} = -F_1 \widehat{y_1} |B1\rangle\langle B1| - F_2 \widehat{y_2} |B2\rangle\langle B2|. \tag{19}$$

The tunneling process $|D; v_i\rangle \rightarrow |A; v_f\rangle$, where $|v_i\rangle = |n(y_1)\rangle|m(y_2)\rangle$ and $|v_f\rangle = |n'(y_1)\rangle|m'(y_2)\rangle$, is now described by the vibronic tunneling matrix element $\langle D; n(y_1)m(y_2)|\hat{T}|A; n'(y_1)m'(y_2)\rangle$. Using Equation 4, one can show that the exchange of energy between the electron and the vibrations identifies the electronic path traversed by the electron. The reason is that, in this model, the vibrations are pathway specific (12, 71). Any elastic tunneling matrix element is the sum over the parallel pathway contributions (here, $B1$ and $B2$), which interfere coherently, e.g., $\langle D; 0(y_1), 0(y_2)|\hat{T}|A; 0(y_1), 0(y_1)\rangle = Path(B1) + Path(B2)$. An inelastic matrix element, such as $\langle D; 1(y_1), 0(y_2)|\hat{T}|A; 0(y_1), 0(y_2)\rangle$, comprises only $Path(B1)$ (12, 71). Therefore, inelastic tunneling can erase the interference among coupling pathways; it is possible that such effects are relevant to protein ET (17). Recent studies have shown that, in a system in which elastic tunneling pathways interfere destructively and ET is symmetry forbidden, the enhancement of inelastic tunneling induced by exciting bridge vibrational modes with infrared irradiation can switch on ET (72). The field of inelastic tunneling ET reactions is closely related to inelastic tunneling spectroscopy (e.g., see 73, 74; reviewed in 75, 76).

A UNIMOLECULAR WHICH-WAY INTERFEROMETER

Leaving spatially localized vibrational energy behind on (or picking it up from) a tunneling pathway records the route that the electron traversed. Knowing this route with certainty removes all coupling pathways that do not include that specific coupling step (i.e., the group in which the vibrational energy was deposited) from the pathway sum (12). Figure 6 illustrates the concept of a molecular which-way interferometer. The key element is that spatially localized and distinguishable normal modes couple to bridge sites. Experiments to test these ideas are employing infrared excitation of bridge vibrational modes in a three-color experiment (77).

5. SOLVENT CONTROL OF ELECTRON TRANSFER

In the above sections, we explore nonadiabatic ET, in which the rate is limited by electron tunneling and tunneling fluctuations. It is well-known that for adiabatic ET, the rate-limiting step may be solvent relaxation, and the solvent fluctuation timescale becomes particularly important (1–7). The importance of solvent dynamics in the intermediate to nonadiabatic limits has not been well appreciated, however. Recent studies of the transition from solvent polarization control to tunneling control of ET, using the U-shaped molecules shown in Figure 7, are elucidating the relevant timescale considerations for such ET processes.

For the U-shaped molecules shown in Figure 7, T_{DA} is smaller than k_BT, but not that much smaller, and it is possible to observe a change in ET mechanism by changing the solvent friction. Three different limiting regimes, or mechanisms, are observed in ET reactions: nonadiabatic ET, adiabatic ET, and solvent-controlled ET. Criteria for transitions between the adiabatic and nonadiabatic regime are related to the nature of the nuclear motion through the crossing (e.g., ballistic or overdamped) and can be formulated in terms of the Landau-Zener curve-crossing problem (1–7). In the nonadiabatic case (discussed in the previous sections), the electronic coupling is very weak in the sense that the system has to move through the curve-crossing region many times before the electronic state changes from the donor to the acceptor (see Figure 1). In the discussion that follows, we use Equation 11 for the nonadiabatic rate constant and denote the nonadiabatic rate k_{NA} rather than k_{ET}. Furthermore, we assume that in addition to the classical mode that modulates the DA energy gap (U_D and U_A in Figure 1), there is a high-frequency quantum mode that also modulates the gap (with reorganization energy $\tilde{\lambda}$ and frequency $\omega = 2\pi\tilde{\nu}$). In this case the Franck-Condon factor has both classical mode and quantum mode contributions, and the nonadiabatic rate constant becomes

$$k_{NA}=\frac{4\pi^2}{h}\left\langle T_{DA}^2\right\rangle \frac{1}{\sqrt{4\lambda\pi k_B T}}\sum_{n=0}^{\infty}\exp(-S)\left(\frac{S^n}{n!}\right)\exp\left[-\frac{(\Delta G+\lambda+nh\tilde{\nu})^2}{4\lambda k_B T}\right], \tag{20}$$

where λ is the reorganization energy of the classical mode of Figure 1 ($\Delta G=U_A^{\min}-U_D^{\min}$), and $S=\tilde{\lambda}/h\tilde{\nu}$ is the Huang-Rhys factor associated with the reorganization energy and frequency of the quantum mode (1–7). Equation 20 assumes that the initial vibrational state of the quantum mode is the ground state (i.e., $h\tilde{\nu} \gg k_BT$). The Franck-Condon factor in Equation 20 is similar to $\rho_{FC}(\nu_i \rightarrow \nu_f)$ of Equation 16. Both Franck-Condon factors describe the exchange of energy between the electron and quantum vibrations of the system. In Equation 16 the vibrations modulate the DA coupling, whereas in Equation 20, they modulate the DA energy gap (8,65).

In the adiabatic case of large coupling, the reaction proceeds by nuclear motion through the transition state on a single electronic potential energy surface (the lower adiabatic energy surface arising from the coupling T_{DA} between U_D and U_A in Figure 1). The effect of T_{DA} on the rate constant is manifest only through its role in determining the adiabatic surface energy barrier, which is less than E_{act} of Figure 1. In the solvent-controlled limit, the electronic coupling may still be small; however, the rate constant is affected by frictional coupling. In this case, the characteristic time spent in the curve-crossing region is long enough that the electronic state changes from *D* to *A* for nearly every approach to the DA crossing, even though the coupling is weak. Hence the reaction appears adiabatic in the sense that the rate is limited by nuclear dynamics rather than by the electron-tunneling probability.

Zusman (78,79) generalized the rate constant expression for ET, k_{ET}, to describe a transition between the normal nonadiabatic limit k_{NA} and a solvent-controlled limit k_{SC}, namely

$$\frac{1}{k_{ET}}=\frac{1}{k_{SC}}+\frac{1}{k_{NA}}, \tag{21}$$

which shows that the measured ET rate k_{ET} can be limited by either the electronic motion (where k_{NA} is small) or the nuclear motion (when k_{SC} is small). The slower process is rate controlling. In the classical limit he found

$$k_{SC}=\frac{1}{\tau_S}\sqrt{\frac{\lambda}{\pi^3 k_B T}}\sin\left(\pi\sqrt{\frac{\Delta G^{\neq}}{\lambda}}\right)\exp\left(-\frac{\Delta G^{\neq}}{\lambda}\right), \quad (22)$$

in which the ET rate is proportional to the solvation rate, $1/\tau_s$, where τ_s is the solvation time. It is the characteristic time that it takes for the solvent to respond to a change in the charge distribution of a solute and has been quantified in a number of different ways (vide infra). In Equation 22, $\Delta G^{\neq} = (\Delta G + \lambda)^2/4\lambda$ (in the notation of Figure 1, $\Delta G \to U_A^{\min} - U_D^{\min}$ and $\Delta G^{\neq} \to E_{act}$). Because the solvation time τ_s increases dramatically with decreasing temperature, especially in viscous solvents, the solvation time becomes more important as the temperature is lowered. Zusman used the inequality

$$\frac{\pi^2|T_{DA}|^2\tau_S}{\hbar\lambda_0}\exp(-S) \gg \left(\sin\frac{\pi}{2}\left(\frac{\Delta G}{\lambda}+1\right)\right) \quad (23)$$

to assess when the solvent friction should be important for the ET rate. In the context of our previous discussion of fluctuating DA couplings, $|T_{DA}|$ in Equation 23 should be interpreted as $T_{DA}^{rms}=\sqrt{\langle T_{DA}^2\rangle}$. For small driving forces, $|\Delta G| \ll \lambda$, this criterion is $\frac{\pi^2\tau_S|T_{DA}^{eff}|^2}{\hbar\lambda} \gg 1$, where $|T_{DA}^{eff}|=|T_{DA}|\exp(-S/2)$. Hence, the solvent-controlled regime may be interpreted to arise from a solvent-driven change of adiabaticity, characterized by an adiabaticity parameter *g*, where (80)

$$g=\frac{|T_{DA}^{eff}|^2\pi^2\tau_S}{\hbar\lambda}. \quad (24)$$

When $g \gg 1$, the reaction is solvent controlled, and when $g \ll 1$, it is nonadiabatic.

In addition to Zusman's model, there have been several theoretical approaches to the problem of solvent-controlled ET and to the transition from nonadiabatic to adiabatic ET [e.g., for reviews, see Calef & Wolynes (81), Morillo & Cukier (82) Hynes (83), Sumi and Marcus (84), Onuchic and coworkers (86), Sparpaglione & Mukamel (87,88), Rips & Jortner (89), and Jortner & Bixon (4)]. Sumi & Marcus (84) considered the combined effects of intramolecular vibrations and diffusive solvent orientational motions on ET. They described the reaction as proceeding along a two-dimensional effective potential energy surface, $V(q, X)$. The coordinate *X* corresponds to the solvent polarization (the polarization response of the solvent to changes of the charge distribution), and *q* is an intramolecular vibrational coordinate, which includes the fast nuclear motions typical of an ET reaction in the nonadiabatic or adiabatic limit. To find the reaction rate, they solved the Fokker-Planck equation for diffusive motion along *X* and treated the motion along *q* through a rate constant $k(X)$ that depends on the fast motions in the normal way (e.g., Equation 1) and depends parametrically on *X* (84,85).

It was found that the electron transfer rate of the U-shaped molecules in Figure 7 in fast solvents (90,91) could be modeled by using Equation 21 with an internal (quantum mode) reorganization energy $\tilde{\lambda}$ of 0.65 eV and an effective quantum mode frequency of 1600 cm^{-1}. Comparison with solvation models indicated that the solvent (classical mode) reorganization energy λ was between 1.2 eV and 1.4 eV for molecules 1 and 2 in Figure 7 in NMA (N-methylacetamide) and NMP (N-methylpropionamide) (vide infra). The ratio $\tilde{\lambda}/\lambda$ is thus approximately 0.5, which

places these reactions in the narrow reaction window limit of Sumi & Marcus (84). This limit is also one in which Zusman's predictions (Equations 21 and 22) should apply. Sumi & Marcus pointed out the nonexponential character in the narrow reaction window limit; however, Zusman's treatment does not address this feature.

By studying chemical systems in different solvents with a range of solvent relaxation times, Waldeck and coworkers (29,85,92,93) explored the limit in which the ET time $\tau_{ET} = 1/k_{ET}$ is controlled by τ_s, which is commonly modeled by a characteristic dielectric relaxation (Debye) time (79) or the characteristic time measured in a dynamic Stokes shift experiment (94). They reported a transition from the nonadiabatic ET regime to the solvent-controlled limit and showed how it depends on the solvent relaxation time and the electronic coupling strength. The molecules shown in Figure 7 (molecules 1, 2, and 3) have empirically determined electronic couplings in the range of tens to hundreds of wave numbers (depending on the pendant group that is placed in the cleft). In solvents with rapid polarization fluctuations, as measured by their dynamic Stokes shift relaxation times, the ET followed a first-order (i.e., exponential) rate and proceeded in the nonadiabatic limit. However, in slow solvents (e.g., NMP), the rate displayed a nonexponential behavior that was controlled by the solvent relaxation rate.

Because the rate was nonexponential, Waldeck and coworkers (93,95) defined a rate constant k_{ET} from the inverse of the correlation time for the decay of the reactant state (i.e., the time integral of the temporal profile of the initially excited state), so it was possible to plot the ln $(k_{ET} T^{1/2})$ versus the inverse of the temperature T (see Figure 8). The rate constants for all three compounds were similar at low temperatures and deviate from one another at higher temperatures. The deviation occurred first for compound 1 (at 260 K to 270 K; NMP solvation time of approximately 240 ps) and then for compounds 2 and 3 at higher temperature (above 310 K; NMP solvation time of approximately 55 ps). Thus, the trend in characteristic times for the different solutes correlated with the change in electronic coupling $|T_{DA}|$ (see Table 1) that was determined for these three molecules in aromatic solvents and acetonitrile, which have a rapid solvation response (τ_s is small).

The data in Figure 8 show that the ET rate of compound 2 is higher than that of compound 3 in NMP, and compound 1 has the lowest ET rate. This trend is reflected in the electronic coupling values extracted from a fit of the rate data in solvents with a fast solvation response by the semiclassical equation (Equation 20; see Table 1). The electronic coupling magnitude of compound 2 with a methoxy substituted pendant group is the largest among the molecules, and this large value can be rationalized in terms of that group's electron affinity and ionization potential. The reorganization energy and Gibbs free energy parameters in Table 1 vary somewhat among the compounds, but the activation barrier for the reaction $\Delta G^{\neq} = (\Delta G + \lambda)^2/4\lambda$ is similar for the three structures at 295 K (from 0.160 eV to 0.164 eV). The similarity of the activation barriers (and energetic parameters) is consistent with the similar size, shape, and chemical structure of the molecules. This similarity is found even though the rate data appear to deviate substantially from one another as the temperature changes.

The self-consistency of this analysis can be assessed by considering the dependency of the rate constant on the solvation time. The different kinetic models predict that the ET rate constant is inversely proportional to the solvation time in the solvent-controlled regime, but that it becomes independent of solvent friction when the solvation time is short.

Figure 9 plots a reduced ET time τ^*_{ET} (Equation 25), defined in terms of Zusman's timescale (78,96,97) as

$$\tau^*_{ET,Z} = \frac{\sqrt{\pi^3}}{\lambda \sin\left(\pi \sqrt{\frac{\Delta G^{\neq}}{\lambda}}\right)} \tau_S + \frac{\hbar}{\sqrt{\pi}} \frac{1}{|T_{DA}|^2} \quad (25)$$

versus the solvation time of NMP. For all of these molecules, a linear correlation exists between τ^*_{ET} and the solvation time at low temperature, and the ET times become independent of the solvation time at high temperatures. The Sparpaglione-Mukamel treatment (87,88) is similar. Both models fail to predict the observed slopes quantitatively, although they otherwise provide an accurate description of the data. As discussed above, when $g \gg 1$ the reaction is solvent controlled, and when $g \ll 1$ it is nonadiabatic. This analysis predicts that the solvent-controlled regime is reached when $\tau_S \gg 24$ ps for compound 1, $\tau_S \gg 2$ ps for compound 2, and $\tau_S \gg 6$ ps for compound 3 in NMP. The experimental results (Figure 7) indicate that compounds 2 and 3 are in the solvent-controlled limit (coalescence of rates) when τ_S is near 56 ps, and for compound 1 the solvent-controlled limit is reached at around 240 ps. Thus, the trend in the rate data can be understood via the Zusman model.

6. GATED ELECTRON TRANSFER VERSUS DYNAMICAL CONTROL

If any of the timescales discussed above is longer than the ET time, the ET kinetics may be multi-exponential or gated. Figure 10 shows rate constants for cytochrome *c* immobilized in two different ways in monolayer films (electrostatic adsorption and ligation of the iron heme) (98–100). Although the thickness dependencies of the rates are shifted from one another, determined by the immobilization, both tethering schemes show an exponential distance dependence for thick films and a weaker distance dependence for thin films. A number of studies (101–107) have found a change in the ET reaction mechanism with distance from an electrode for immobilized proteins. For cytochrome *c* immobilized by heme ligation, the tunneling regime is reached for long tethers ($n \geq 12$) and is controlled by medium relaxation for short tethers (98, 108). The soft distance dependence of the rate and its sensitivity to the medium friction can be rationalized in different ways. For a gated mechanism, the conformation changes are slow with respect to the ET time and limit the rate for thin films; i.e., the system fluctuates to a geometry of large DA coupling. Alternatively, the experimental data can be explained by a change in the ET mechanism from nonadiabatic at long distances to solvent controlled at shorter distances.

Yue and coworkers (99) distinguished tunneling control from relaxation control mechanisms by measuring the dependence of the ET rate on the overpotential. For electrostatic assemblies on silver, they found no dependence on the overpotential, indicating that ET is gated. For ligated-protein assemblies on gold electrodes, they found an overpotential dependence, suggesting that ET proceeds in an effective adiabatic/medium-controlled limit. Yue and coworkers (99) also performed a temperature-dependent study of protein ET and found that the activation barrier has contributions from both the ET reorganization energy and the medium friction's apparent activation. These findings suggest that the so-called unusual distance dependence of the heterogeneous ET rate, reported for different proteins immobilized on metals, may be explained by the same underlying principles.

7. CONCLUSIONS AND PROSPECTS

Molecular fluctuations in ET systems not only enable access to the activated complex, but also cause DA electronic interactions to fluctuate. The magnitudes and timescales of these fluctuations can determine the reaction mechanism. The interplay among electronic coupling and nuclear fluctuations is particularly important in biological electron transfer because protein

and water bridges dominate the electron-tunneling pathways. Simulations indicate that the Condon approximation appears to be valid for most of the proteins studied so far. For long-range ET, the rates tend to be controlled by fluctuations of the coupling away from its mean value. Indeed, because of destructive interferences among multiple paths, the mean coupling value tends to be quite small. Small-molecule studies show that solvent relaxation can change the adiabaticity of ET and, for highly sluggish solvents, limit the ET rate even for intermediate (approximately 100 cm^{-1}) couplings. Such effects are expected to be important for proteins in which a wide distribution of relaxation processes and timescales are present (see 109). Electrochemical studies of immobilized proteins are being used to reveal how the ET rate changes from the tunneling limit to relaxation control. Electron tunneling, gated ET, and solvent relaxation controlled ET are now well documented in both small-molecule and protein systems alike.

It is clear that inelastic tunneling, in addition to modifying the free energy dependence of ET kinetics, could have substantial effects on coupling pathway interferences. The quantitative theoretical framework that has emerged from these recent studies suggests that one may now be able to formulate general principles linking the structure, fluctuations, and function with ET kinetics. This framework also appears likely to frame new questions in molecular biophysical chemistry. For example, single-molecule studies of ET suggest the possibility of directly probing the role of fluctuations in ET reactions experimentally. Xie and colleagues (110) have reported measurements of ET in a flavoprotein, and Barbara and coworkers (111) have reported single-molecule measurements of ET at electrodes. Studies of this kind in systems with structural flexibility offer the opportunity to explore, in great detail, the role of fluctuations in bioenergetics. Indeed, Rubtsov and coworkers (77) just reported an ultrafast multipulse experiment that uses infrared excitation to perturb electron DA interactions during the course of an ET reaction.

FUTURE ISSUES

1. Experimental probes of pathway coherence, including inelastic labeling of paths, should be developed.
2. Experiments should be designed that are directly sensitive to coupling fluctuations.
3. Electron tunneling across organized water structures needs to be investigated.
4. Experiments should be designed that access multiple ET regimes in single systems: few-path tunneling, multipath tunneling, fluctuation-controlled tunneling, protein-gated tunneling, solvent relaxation limited transport, and carrier injection limited transport.

Glossary

ET	electron transfer
T_{DA}	tunneling matrix element
$\sigma_{T_{DA}}$	variance of the tunneling matrix element
R_{coh}	coherence parameter
NMP	N-methylpropionamide

Acknowledgments

S.S.S. thanks the University of Cyprus, D.H.W. thanks the NSF (CHE-0718755), and D.N.B. thanks the NSF (CHE-0718043) and the NIH (GM-48043) for support of these research activities.

LITERATURE CITED

1. Marcus RA, Sutin N. Electron transfers in chemistry and biology. Biochim. Biophys. Acta 1985;811:265–322.
2. Jortner, J.; Ratner, MA. Molecular Electronics. Oxford: Blackwell Science; 1997.
3. Kuznetsov, AM.; Ulstrup, J. Electron Transfer in Chemistry and Biology. Chichester, UK: Wiley; 1999.
4. Jortner, J.; Bixon, M., editors. Electron Transfer: From Isolated Molecules to Biomolecules. Adv. Chem. Phys. Ser. New York: Wiley Intersci.; 1999. p. 106-107.
5. May, V.; Kuhn, O. Charge and Energy Transfer Dynamics in Molecular Systems. Berlin: Wiley-VCH; 2000.
6. Balzani, V.; Piotrowiak, P.; Rodgers, MAJ.; Mattay, J.; Astruc, D., et al. Electron Transfer in Chemistry. Vol. Vols. I–V. Weinheim: Wiley-VCH; 2001.
7. Nitzan, A. Chemical Dynamics in Condensed Phases. Oxford: Oxford Univ. Press; 2006.
8. Troisi A, Nitzan A, Ratner MA. A rate constant expression for charge transfer through fluctuating bridges. J. Chem. Phys 2003;119:5782–5788.
9. Skourtis, SS.; Lin, J.; Beratan, DN. The effects of bridge motion on electron transfer reactions mediated by tunneling. In: Starikov, EB.; Lewis, JP.; Tanaka, S., editors. Modern Methods for Theoretical Physical Chemistry of Biopolymers. Boston: Elsevier; 2006. p. 357-382.
10. Skourtis SS, Beratan DN, Onuchic JN. The two-state reduction for electron and hole transfer in bridge-mediated electron-transfer reactions. Chem. Phys 1993;176:501–520.
11. Skourtis SS, Beratan DN. Theories of structure-function relationships for bridge-mediated electron transfer reactions. Adv. Chem. Phys 1999;106:377–452.
12. Skourtis SS, Waldeck DH, Beratan DN. Inelastic electron tunneling erases coupling-pathway interferences. J. Phys. Chem. B 2004;108:15511–15518.
13. Teklos A, Skourtis SS. Comparative studies of perturbative methods for computing electron transfer tunneling matrix elements for a nonorthogonal basis set. J. Chem. Phys 2006;125:244103–244109. [PubMed: 17199336]
14. Xie Q, Archontis G, Skourtis SS. Protein electron transfer: a numerical study of tunneling through fluctuating bridges. Chem. Phys. Lett 1999;312:237–246.
15. Skourtis SS, Archontis G, Xie Q. Electron transfer through fluctuating bridges: on the validity of the superexchange mechanism and time-dependent tunneling matrix elements. J. Chem. Phys 2001;115:9444–9462.
16. Cave RJ, Newton MD. Generalization of the Mulliken-Hush treatment for the calculation of electron transfer matrix elements. Chem. Phys. Lett 1996;249:15–19.
17. Stuchebrukhov AA. Toward ab initio theory of long-distance electron tunneling in proteins: tunneling currents approach. Adv. Chem. Phys 2001;118:1–44.
18. Troisi A, Ratner MA, Zimmt MB. Dynamic nature of the intramolecular electronic coupling mediated by a solvent molecule: a computational study. J. Am. Chem. Soc 2004;126:2215–2224. [PubMed: 14971957]
19. Skourtis SS, Balabin IA, Kawatsu T, Beratan DN. Protein dynamics and electron transfer: electronic decoherence and non-Condon effects. Proc. Natl. Acad. Sci. USA 2005;102:3552–3557. [PubMed: 15738409]
20. Balabin IA, Onuchic JN. Dynamically controlled protein tunneling paths in photosynthetic reaction centers. Science 2000;290:114–117. [PubMed: 11021791]
21. Nishioka H, Kimura A, Yamato T, Kawatsu T, Kakitani T. Interference, fluctuation, and alternation of electron tunneling in protein media. 2. Non-Condon theory for the energy gap dependence of electron transfer rate. J. Phys. Chem. B 2005;109:15621–15635. [PubMed: 16852980]

22. Bixon M, Jortner J. Effects of configurational fluctuation on electronic coupling for charge transfer dynamics. Russ. J. Electrochem 2003;39:3–8.
23. Berlin YA, Grozema FC, Siebbeles LDA, Ratner MA. Charge transfer in donor-bridge-acceptor systems: static disorder, dynamic fluctuations, and complex kinetics. J. Phys. Chem. C 2008;112:10988–11000.
24. Jordan KD, Paddon-Row MN. Analysis of the interactions responsible for long-range through-bond-mediated electronic coupling between remote chromophores attached to rigid polynorbornyl bridges. Chem. Revs 1992;92:395–410.
25. Jordan KD, Paddon-Row MN. Long-range interactions in a series of rigid nonconjugated dienes. 1. Distance dependence of the π^+, π^- and π^* splittings determined by ab initio calculations. J. Phys. Chem 1992;96:1188–1196.
26. Curtiss LA, Naleway CA, Miller JR. Superexchange pathway calculation of long-distance electronic coupling in $H_2C(CH_2)M\text{-}2CH_2$ chains. Chem. Phys 1993;176:387–405.
27. Liang CX, Newton MD. Ab initio studies of electron transfer: pathway analysis of effective transfer integrals. J. Phys. Chem 1992;96:2855–2866.
28. Newton MD. Modeling donor/acceptor interactions: combined roles of theory and computation. Int. J. Quantum Chem 2000;77:255–263.
29. Chakrabarti S, Liu M, Waldeck DH, Oliver AM, Paddon-Row MN. Solvent dynamical effects on electron transfer in U-shaped donor-bridge-acceptor molecules. J. Phys. Chem. A 2009;113:1040–1048. [PubMed: 19146395]
30. Kumar K, Lin Z, Waldeck DH, Zimmt MB. Electronic coupling in C-clamp-shaped molecules: solvent-mediated superexchange pathways. J. Am. Chem. Soc 1996;118:243–244.
31. Read I, Napper A, Kaplan R, Zimmt MB, Waldeck DH. Solvent-mediated electronic coupling: the role of solvent placement. J. Am. Chem. Soc 1999;121:10976–10986.
32. Napper AM, Read I, Waldeck DH, Kaplan RW, Zimmt MB. Electron transfer reactions of C-shaped molecules in alkylated aromatic solvents: evidence that the effective electronic coupling magnitude is temperature-dependent. J. Phys. Chem. A 2002;106:4784–4793.
33. Zimmt MB, Waldeck DH. Exposing solvent's roles in electron transfer reactions: tunneling pathway and solvation. J. Phys. Chem. A 2003;107:3580–3597.
34. Wolfgang J, Risser SM, Priyadarshy S, Beratan DN. Secondary structure conformations and long range electronic interactions in oligopeptides. J. Phys. Chem. B 1997;101:2986–2991.
35. Daizadeh I, Medvedev ES, Stuchebrukhov AA. Effect of protein dynamics on biological electron transfer. Proc. Natl. Acad. Sci. USA 1997;94:3703–3708. [PubMed: 9108041]
36. Ungar LW, Newton MD, Voth GA. Classical and quantum simulation of electron transfer through a polypeptide. J. Phys. Chem. B 1999;103:7367–7382.
37. Miller NE, Wander MC, Cave RJ. A theoretical study of the electronic coupling element for electron transfer in water. J. Phys. Chem. A 1999;103:1084–1093.
38. Castner EW, Kennedy D, Cave RJ. Solvent as electron donor: Donor/acceptor electronic coupling is a dynamical variable. J. Phys. Chem. A 2000;104:2869–2885.
39. Troisi A, Orlandi G. Hole migration in DNA: a theoretical analysis of the role of structural fluctuations. J. Phys. Chem. B 2002;106:2093–2101.
40. Kawatsu T, Kakitani T, Yamato T. Destructive interference in the electron tunneling through protein media. J. Phys. Chem. B 2002;106:11356–11366.
41. Lockwood DM, Cheng YK, Rossky PJ. Electronic decoherence for electron transfer in blue copper proteins. Chem. Phys. Lett 2001;345:159–165.
42. Warshel A, Chu ZT, Parson WW. Dispersed polaron simulations of electron transfer in photosynthetic reaction centers. Science 1989;246:112–116. [PubMed: 2675313]
43. Warshel A, Parson WW. Dynamics of biochemical and biophysical reactions: insight from computer simulations. Q. Rev. Biophys 2001;34:563–679. [PubMed: 11852595]
44. Teklos A, Skourtis SS. Electron transfer through time dependent bridges: differences between Franck-Condon and Born-Oppenheimer breakdown. Chem. Phys 2005;319:52–68.
45. Balabin IA, Beratan DN, Skourtis SS. Persistence of structure over fluctuations in biological electron-transfer reactions. Phys. Rev. Lett 2008;101:158102. [PubMed: 18999647]

46. Gray HB, Winkler JR. Electron tunneling through proteins. Q. Rev. Biophys 2003;36:341–372. [PubMed: 15029828]
47. Lin JP, Balabin IA, Beratan DN. The nature of aqueous tunneling pathways between electron-transfer proteins. Science 2005;310:1311–1313. [PubMed: 16311331]
48. Prytkova TR, Kurnikov IV, Beratan DN. Coupling coherence distinguishes structure sensitivity in protein electron transfer. Science 2007;315:622–625. [PubMed: 17272715]
49. Beratan DN, Betts JN, Onuchic JN. Protein electron-transfer rates set by the bridging secondary and tertiary structure. Science 1991;252:1285–1288. [PubMed: 1656523]
50. Beratan DN, Skourtis SS, Balabin IA, Balaeff A, Keinan S, et al. Steering electrons on moving pathways. Accounts Chem. Res 2009;42:1669–1678.
51. Edwards PP, Gray HB, Lodge MTJ, Williams RJP. Electron transfer and electronic conduction through an intervening medium. Angew. Chem. Int. Ed. Engl 2008;47:6758–6765. [PubMed: 18651676]
52. Onuchic JN, Kobayashi C, Miyashita O, Jennings P, Baldridge KK. Exploring biomolecular machines: energy landscape control of biological reactions. Philos. Trans. R. Soc. Lond. Ser. B 2006;361:1439–1443. [PubMed: 16873130]
53. Moser CC, Page CC, Dutton PL. Darwin at the molecular scale: selection and variance in electron tunnelling proteins including cytochrome *c* oxidase. Philos. Trans. R. Soc. Lond. Ser. B 2006;361:1295–1305. [PubMed: 16873117]
54. Jones ML, Kurnikov IV, Beratan DN. The nature of tunneling pathway and average packing density models for protein-mediated electron transfer. J. Phys. Chem. A 2002;106:2002–2006.
55. Schuster, GB., editor. Topics in Current Chemistry. Vol. Vols. 236–237. Berlin: Springer; 2004.
56. Skourtis SS. Electron transfer through time-dependent bridges: tunneling by virtual transitions that break the Born-Oppenheimer approximation. Chem. Phys. Lett 2003;372:224–231.
57. Hatcher E, Balaeff A, Keinan S, Venkatramani R, Beratan DN. PNA versus DNA: effects of structural fluctuations on electronic structure and hole-transport mechanisms. J. Am. Chem. Soc 2008;130:11752–11761. [PubMed: 18693722]
58. Gutierrez R, Caetano RA, Woiczikowski BP, Kubar T, Elstner M, Cuniberti G. Charge transport through biomolecular wires in a solvent: bridging molecular dynamics and model Hamiltonian approaches. Phys. Rev. Lett 2009;102:208102. [PubMed: 19519078]
59. Woiczikowski PB, Kubar T, Gutierrez R, Caetano RA, Cuniberti G, Elstner M. Combined density functional theory and Landauer approach for hole transfer in DNA along classical molecular dynamics trajectories. J. Chem. Phys 2009;130:215104. [PubMed: 19508103]
60. Onuchic JN, DaGama AAS. Influence of intersite modes on the exchange interaction in electron-transfer at large distances. Theor. Chim. Acta 1986;69:89–100.
61. Mikkelsen KV, Ulstrup J, Zakaraya MG. Free-energy dependence of the electronic factor in biological long-range electron transfer. J. Am. Chem. Soc 1989;111:1315–1319.
62. Goldstein RF, Franzen S, Bialek W. Nonperturbative approach to non-Condon effects: Must a nonadiabatic transition always occur at the potential surface crossing? J. Phys. Chem 1993;97:11168–11174.
63. Tang J. Effects of a fluctuating electronic coupling on electron-transfer rate. J. Chem. Phys 1993;98:6263–6266.
64. Goychuk IA, Petrov EG, May V. Bridge-assisted electron-transfer driven by dichotomically fluctuating tunneling coupling. J. Chem. Phys 1995;103:4937–4944.
65. Medvedev ES, Stuchebrukhov AA. Inelastic tunneling in long-distance biological electron transfer reactions. J. Chem. Phys 1997;107:3821–3831.
66. Liao JL, Voth GA. Numerical approaches for computing nonadiabatic electron transfer rate constants. J. Chem. Phys 2002;116:9174–9187.
67. Milischuk A, Matyushov DV. Non-Condon theory of nonadiabatic electron transfer reactions in V-shaped donor-bridge-acceptor complexes. J. Chem. Phys 2003;118:5596–5606.
68. Jang SJ, Newton MD. Theory of torsional non-Condon electron transfer: a generalized spin-boson Hamiltonian and its nonadiabatic limit solution. J. Chem. Phys 2005;122:024501. [PubMed: 15638592]

69. Rehm D, Weller A. Kinetics of fluorescence quenching by electron and H-atom transfer. Isr. J. Chem 1970;8:259–271.
70. Mines GA, Bjerrum MJ, Hill MG, Casimiro DR, Chang IJ, et al. Rates of heme oxidation and reduction in Ru(His33)cytochrome *c* at very high driving forces. J. Am. Chem. Soc 1996;118:1961–1965.
71. Skourtis SS, Beratan DN. A molecular double slit paradigm. AIP Conf. Proc 2007;963:809–812.
72. Xiao D, Skourtis SS, Rubtsov IV, Beratan DN. Turning charge transfer on and off in a molecular interferometer with vibronic pathways. Nano Lett 2009;9:1818–1823. [PubMed: 19435376]
73. Maddox JB, Harbola U, Liu N, Silien C, Ho W, et al. Simulation of single molecule inelastic electron tunneling signals in paraphenylene-vinylene oligomers and distyrylbenzene[2.2]paracyclophanes. J. Phys. Chem. A 2006;110:6329–6338. [PubMed: 16686469]
74. Troisi A, Beebe JM, Picraux LB, van Zee RD, Stewart DR, et al. Tracing electronic pathways in molecules by using inelastic tunneling spectroscopy. Proc. Natl. Acad. Sci. USA 2007;104:14255–14259. [PubMed: 17726099]
75. Galperin M, Ratner MA, Nitzan A. Molecular transport junctions: vibrational effects. J. Phys. Condens. Matter 2007;19:103201.
76. Kohler S, Lehmann J, Hanggi P. Driven quantum transport on the nanoscale. Phys. Rep 2005;406:379–443.
77. Lin Z, Lawrence CM, Xiao D, Kireev VV, Skourtis SS, et al. Modulating unimolecular charge transfer by exciting bridge vibrations. J. Am. Chem. Soc 2009;131:18060–18062. [PubMed: 19928957]
78. Zusman LD. Outer-sphere electron transfer in polar solvents. Chem. Phys 1980;49:295–304.
79. Zusman LD. Dynamical solvent effects in electron-transfer reactions. Z. Phys. Chem 1994;186:1–29.
80. Beratan DN, Onuchic JN. Adiabaticity and nonadiabaticity in bimolecular outer-sphere charge-transfer reactions. J. Chem. Phys 1988;89:6195–6203.
81. Calef DF, Wolynes PG. Classical solvent dynamics and electron transfer. 1. Continuum theory. J. Phys. Chem 1983;87:3387–3400.
82. Morillo M, Cukier RI. The transition from nonadiabatic to solvent controlled adiabatic electron transfer kinetics: the role of quantum and solvent dynamics. J. Chem. Phys 1988;89:6736–6743.
83. Hynes JT. Outer-sphere electron-transfer reactions and frequency dependent friction. J. Phys. Chem 1986;90:3701–3706.
84. Sumi H, Marcus RA. Dynamic effects in electron-transfer reactions. J. Chem. Phys 1986;84:4894–4914.
85. Liu M, Waldeck DH, Oliver AM, Head NJ, Paddon-Row MN. Observation of dynamic solvent effect for electron tunneling in U-shaped molecules. J. Am. Chem. Soc 2004;126:10778–10786. [PubMed: 15327338]
86. Garg A, Onuchic JN, Ambegaokar J. Effect of friction on electron transfer in biomolecules. J. Chem. Phys 1985;83:4491–4503.
87. Sparpaglione M, Mukamel S. Dielectric friction and the transition from adiabatic to nonadiabatic electron-transfer in condensed phases. 2. Application to non-Debye solvents. J. Chem. Phys 1988;88:4300–4311.
88. Sparpaglione M, Mukamel S. Dielectric friction and the transition from adiabatic to nonadiabatic electron transfer in condensed phases. 1. Solvation dynamics in Liouville space. J. Chem. Phys 1988;88:3263–3280.
89. Rips I, Jortner J. Dynamic solvent effects in outer sphere electron transfer. J. Chem. Phys 1987;87:2090–2104.
90. Napper AM, Read I, Waldeck DH, Head NJ, Oliver AM, Paddon-Row MN. An unequivocal demonstration of the importance of nonbonded contacts in the electronic coupling between electron donor and acceptor units of donor-bridge-acceptor molecules. J. Am. Chem. Soc 2000;122:5220–5221.
91. Napper AM, Head NJ, Oliver AM, Shephard MJ, Paddon-Row MN, et al. Use of U-shaped donor-bridge-acceptor molecules to study electron tunneling through nonbonded contacts. J. Am. Chem. Soc 2002;124:10171–10181. [PubMed: 12188682]

92. Chakrabarti S, Liu M, Waldeck DH, Oliver AM, Paddon-Row MN. Competing electron-transfer pathways in hydrocarbon frameworks: short-circuiting through-bond coupling by nonbonded contacts in rigid U-shaped norbornylogous systems containing a cavity-bound aromatic pendant group. J. Am. Chem. Soc 2007;129:3247–3256. [PubMed: 17315995]

93. Liu M, Ito N, Maroncelli M, Waldeck DH, Oliver AM, Paddon-Row MN. Solvent friction effect on intramolecular electron transfer. J. Am. Chem. Soc 2005;127:17867–17876. [PubMed: 16351118]

94. Maroncelli M. The dynamics of solvation in polar liquids. J. Mol. Liq 1993;57:1–37.

95. Chakrabarti S, Liu M, Waldeck DH, Oliver AM, Paddon-Row MN. Solvent dynamical effects on electron transfer in U-shaped donor-bridge-acceptor molecules. J. Phys. Chem. A 2009;113:1040–1048. [PubMed: 19146395]

96. Zusman L. Dynamical solvent effect in electron-transfer reactions occurring in a mixture of two polar solvents. J. Chem. Phys 1995;102:2580–2584.

97. Zusman LD. Solvent dynamic effects of polarization diffusion in the rate-constant of electron transfer. Electrochim. Acta 1991;36:395–399.

98. Khoshtariya DE, Wei JJ, Liu HY, Yue HJ, Waldeck DH. Charge-transfer mechanism for cytochrome *c* adsorbed on nanometer thick films: distinguishing frictional control from conformational gating. J. Am. Chem. Soc 2003;125:7704–7714. [PubMed: 12812512]

99. Yue HJ, Khoshtariya D, Waldeck DH, Grochol J, Hildebrandt P, Murgida DH. On the electron transfer mechanism between cytochrome *c* and metal electrodes: evidence for dynamic control at short distances. J. Phys. Chem. B 2006;110:19906–19913. [PubMed: 17020376]

100. Yue HJ, Waldeck DH. Understanding interfacial electron transfer to monolayer protein assemblies. Curr. Opin. Solid State Mater 2005;9:28–36.

101. Avila A, Gregory BW, Niki K, Cotton TM. An electrochemical approach to investigate gated electron transfer using a physiological model system: cytochrome *c* immobilized on carboxylic acid-terminated alkanethiol self-assembled monolayers on gold electrodes. J. Phys. Chem. B 2000;104:2759–2766.

102. Niki K, Hardy WR, Hill MG, Li H, Sprinkle JR, et al. Coupling to lysine-13 promotes electron tunneling through carboxylate-terminated alkanethiol self-assembled monolayers to cytochrome *c*. J. Phys. Chem. B 2003;107:9947–9949.

103. Davis KL, Drews BJ, Yue H, Waldeck DH, Knorr K, Clark RA. Electron-transfer kinetics of covalently attached cytochrome *c*/SAM/Au electrode assemblies. J. Phys. Chem. C 2008;112:6571–6576.

104. Murgida DH, Hildebrandt P. Proton-coupled electron transfer of cytochrome *c*. J. Am. Chem. Soc 2001;123:4062–4068. [PubMed: 11457157]

105. Wackerbarth H, Hildebrandt P. Redox and conformational equilibria and dynamics of cytochrome *c* at high electric fields. Chem. Phys. Chem 2003;4:714–724. [PubMed: 12901303]

106. Dolidze TD, Khoshtariya DE, Waldeck DH, Macyk J, van Eldik R. Positive activation volume for a cytochrome *c* electrode process: evidence for a “protein friction” mechanism from high-pressure studies. J. Phys. Chem. B 2003;107:7172–7179.

107. Fujita K, Nakamura N, Ohno H, Leigh BS, Niki K, et al. Mimicking protein-protein electron transfer: voltammetry of *Pseudomonas aeruginosa* azurin and the *Thermus thermophilus* Cu-A domain at ω-derivatized self-assembled-monolayer gold electrodes. J. Am. Chem. Soc 2004;126:13954–13961. [PubMed: 15506756]

108. Wei JJ, Liu HY, Khoshtariya DE, Yamamoto H, Dick A, Waldeck DH. Electron-transfer dynamics of cytochrome *c*: a change in the reaction mechanism with distance. Angew. Chem. Int. Ed. Engl 2002;41:4700–4703. [PubMed: 12481331]

109. LeBard DN, Matyushov DV. Dynamical transition, hydrophobic interface, and the temperature dependence of electrostatic fluctuations in proteins. Phys. Rev. E 2008;78:061901.

110. Yang H, Luo GB, Karnchanaphanurach P, Louie TM, Rech I, et al. Protein conformational dynamics probed by single-molecule electron transfer. Science 2003;302:262–266. [PubMed: 14551431]

111. Palacios RE, Fan FRF, Bard AJ, Barbara PF. Single-molecule spectroelectrochemistry (SMS-EC). J. Am. Chem. Soc 2006;128:9028–9029. [PubMed: 16834364]

RELATED RESOURCES

Bendall, DS., editor. Protein Electron Transfer. Oxford, UK: BIOS Sci.; 1996.

Bertini, I.; Gray, HB.; Stiefel, EI.; Valentine, JS. Bioinorganical Inorganic Chemistry: Structure and Reactivity. Sausalito, CA: Univ. Sci.; 2007.

Gray, HB.; Halpern, J., editors. Proc. Natl. Acad. Sci. USA. Vol. 102. 2005. Long-range electron transfer special feature.

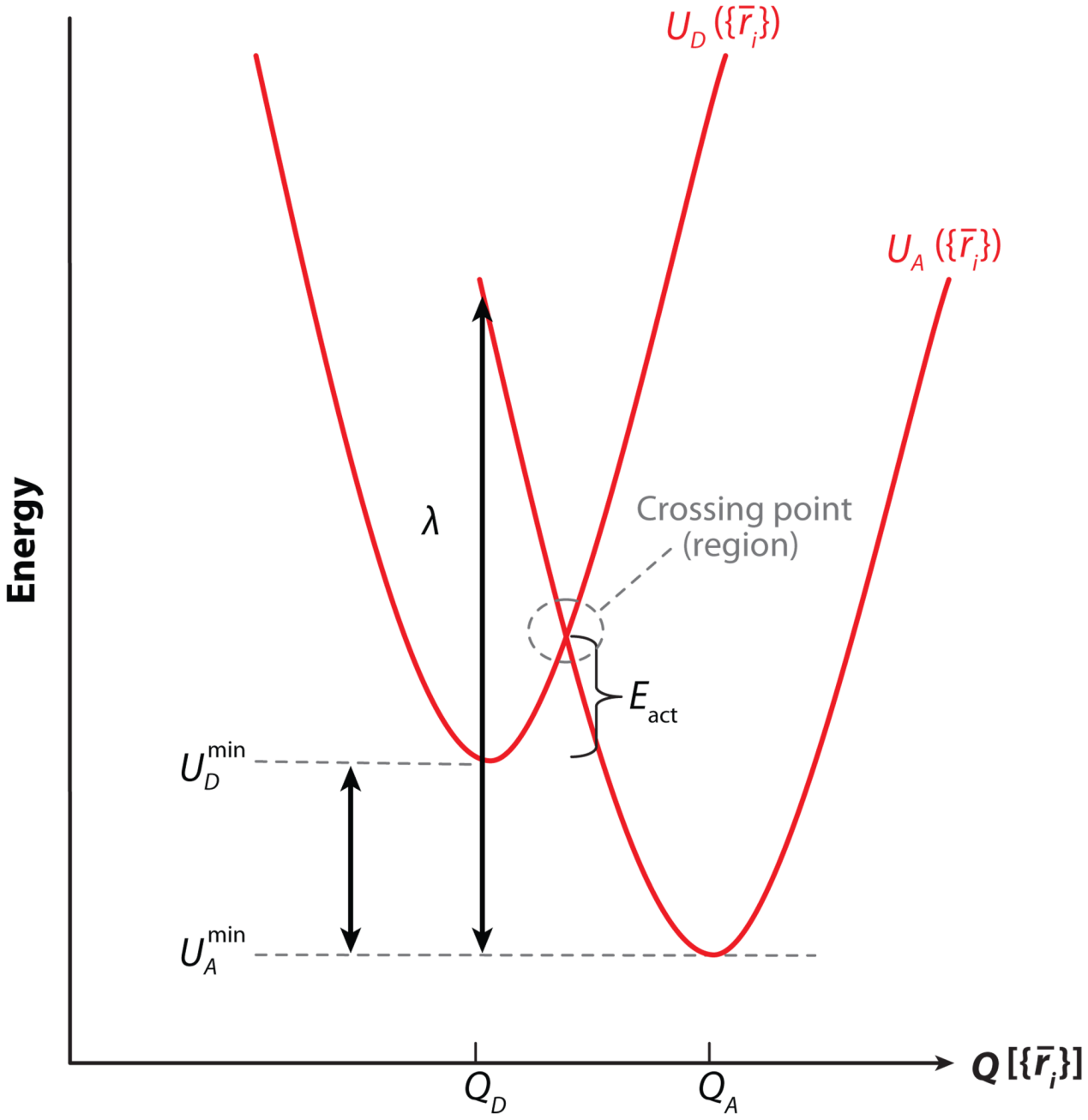

Figure 1.
Donor and acceptor diabatic potential energy curves as a function of the reaction coordinate Q, which is assumed to be a single normal mode ($\{\vec{r}_i\}$ denote atom coordinates). The diagram shows the crossing region, activation energy, energy gap $U_D^{\min} - U_A^{\min}$, and reorganization energy $\lambda = k(Q_D - Q_A)^2/2$, associated with the donor and acceptor potentials (k is the curvature of the surfaces).

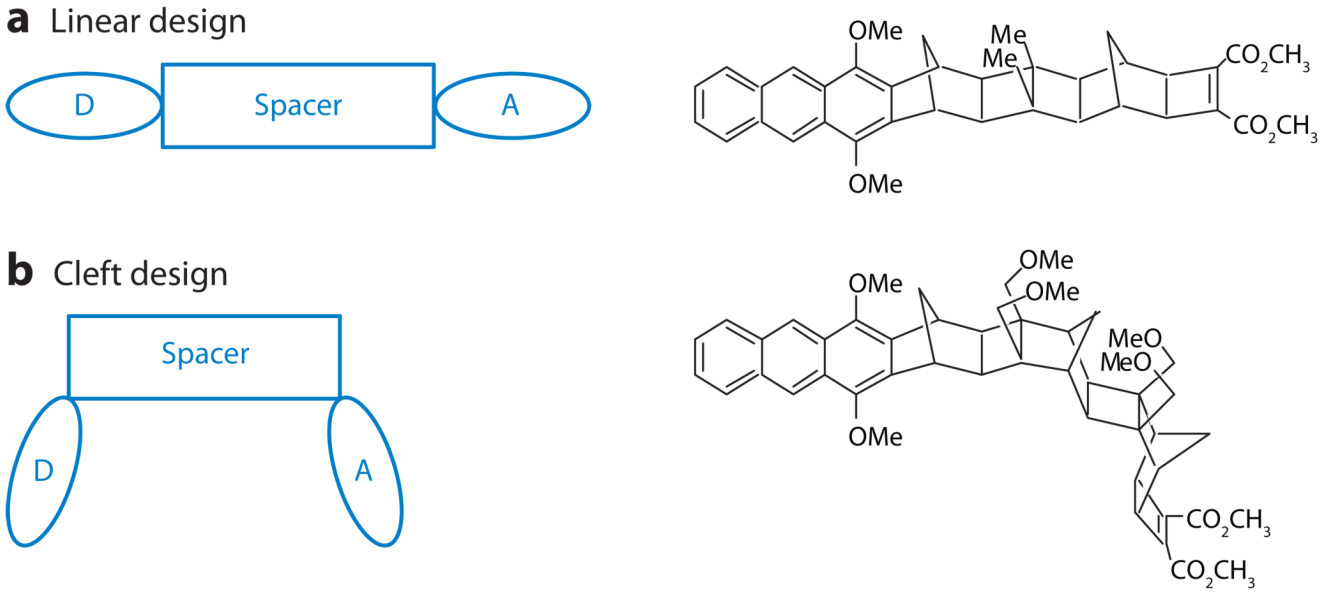

Figure 2.

(*a*) A schematic diagram and example molecular structure for a linear line-of-sight arrangement of donor-bridge-acceptor units in a supermolecule. (*b*) A schematic diagram and example molecular structure for a cleft geometry in which the line of sight between the acceptor and donor is through a gap rather than through a saturated bridge unit.

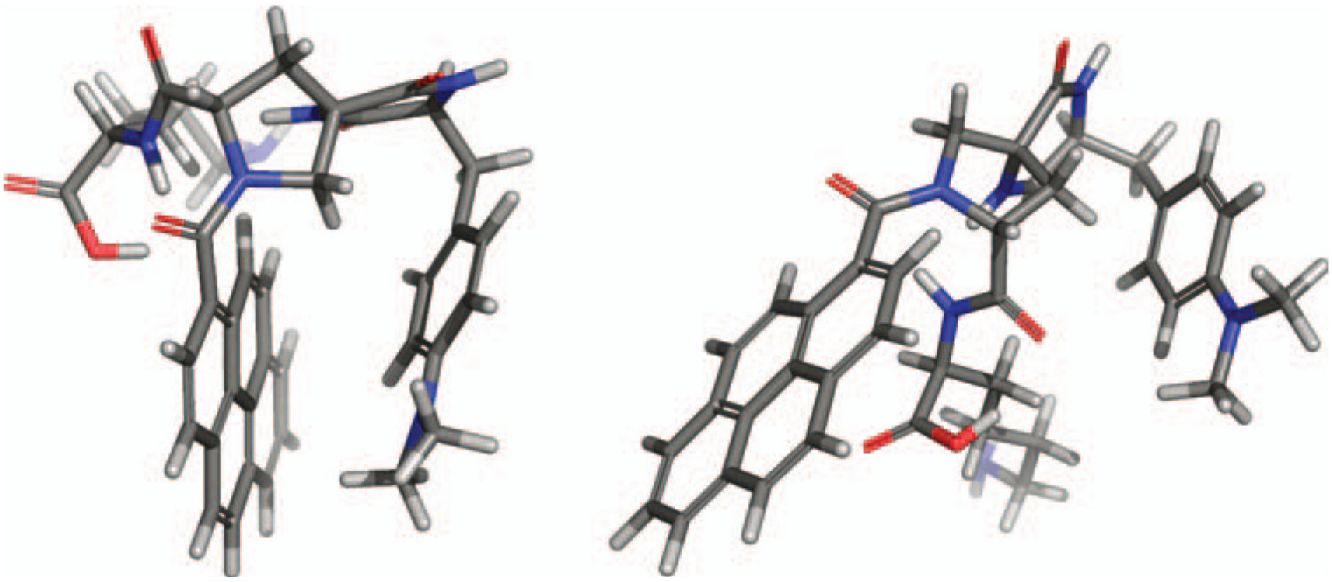

Figure 3.
Molecular structures showing C-clamp molecules with a pyrene acceptor and a dimethylaniline donor. The D-SSS-A supermolecule has a well-defined cleft, whereas the D-SRR-A supermolecule does not.

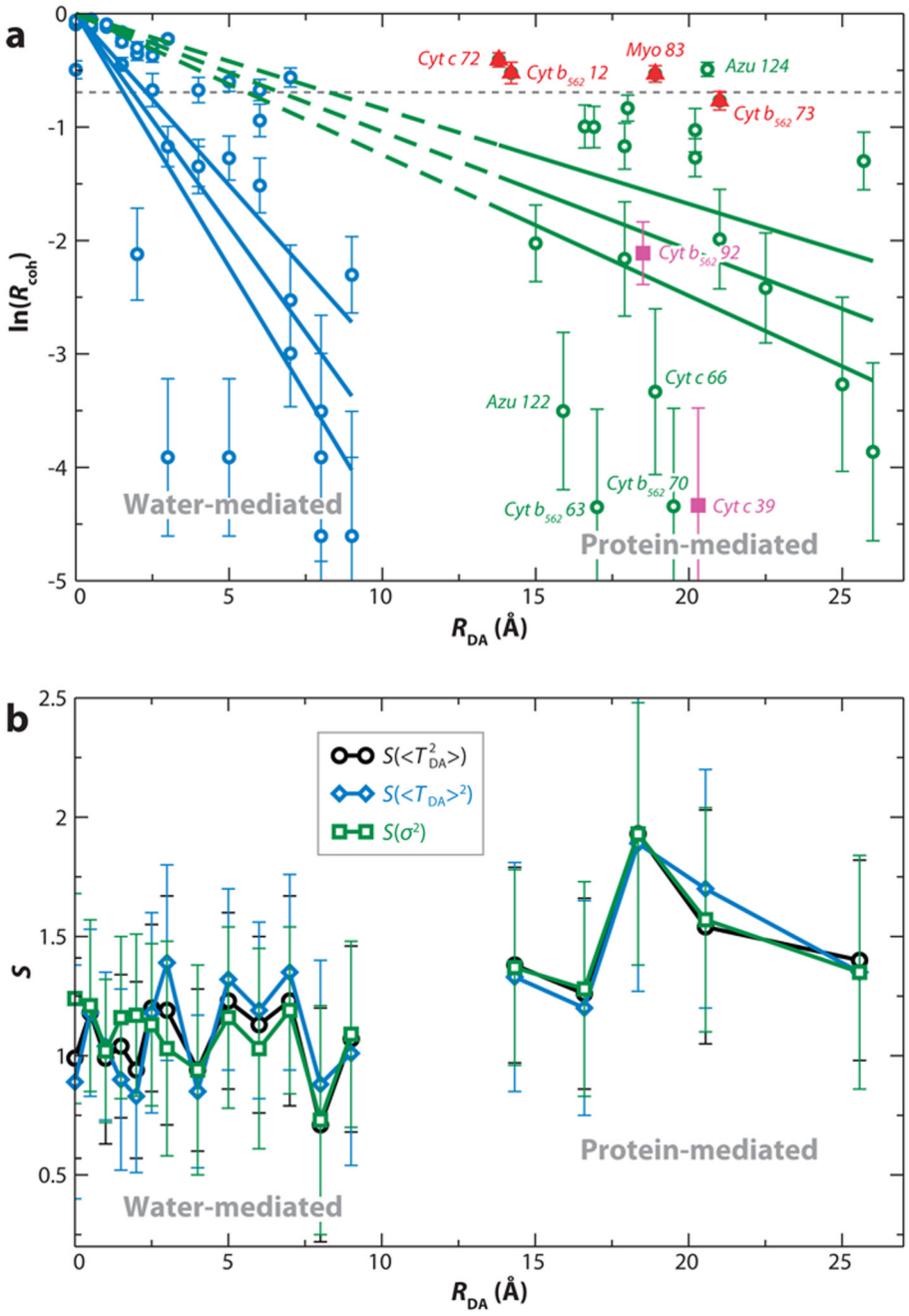

Figure 4.

(*a*) Dependence of ln(R_{coh}) on the donor-acceptor (DA) distance R_{DA}. The vertical lines are error bars, and the horizontal line denotes the value of R_{coh} where $\langle T_{DA}\rangle^2=\sigma^2_{T_{DA}}$, R_{coh}=0.5. (*b*) The scatter function $S_{R_{DA}}(X)=\sqrt{\mathrm{var}[X]R_{DA}}/avg[X]R_{DA}$, where $X=\left\langle T^2_{DA}\right\rangle$ (Equation 14), or $X=\langle T_{DA}\rangle^2, \sigma^2_{T_{DA}}$, is plotted for different R_{DA} distances. An $S_{R_{DA}}$ of the scale of unity indicates that the specific protein structure largely determines the observable rate, whereas $S_{R_{DA}} \ll 1$ means that an effective tunneling barrier could be used to describe the tunneling medium (45).

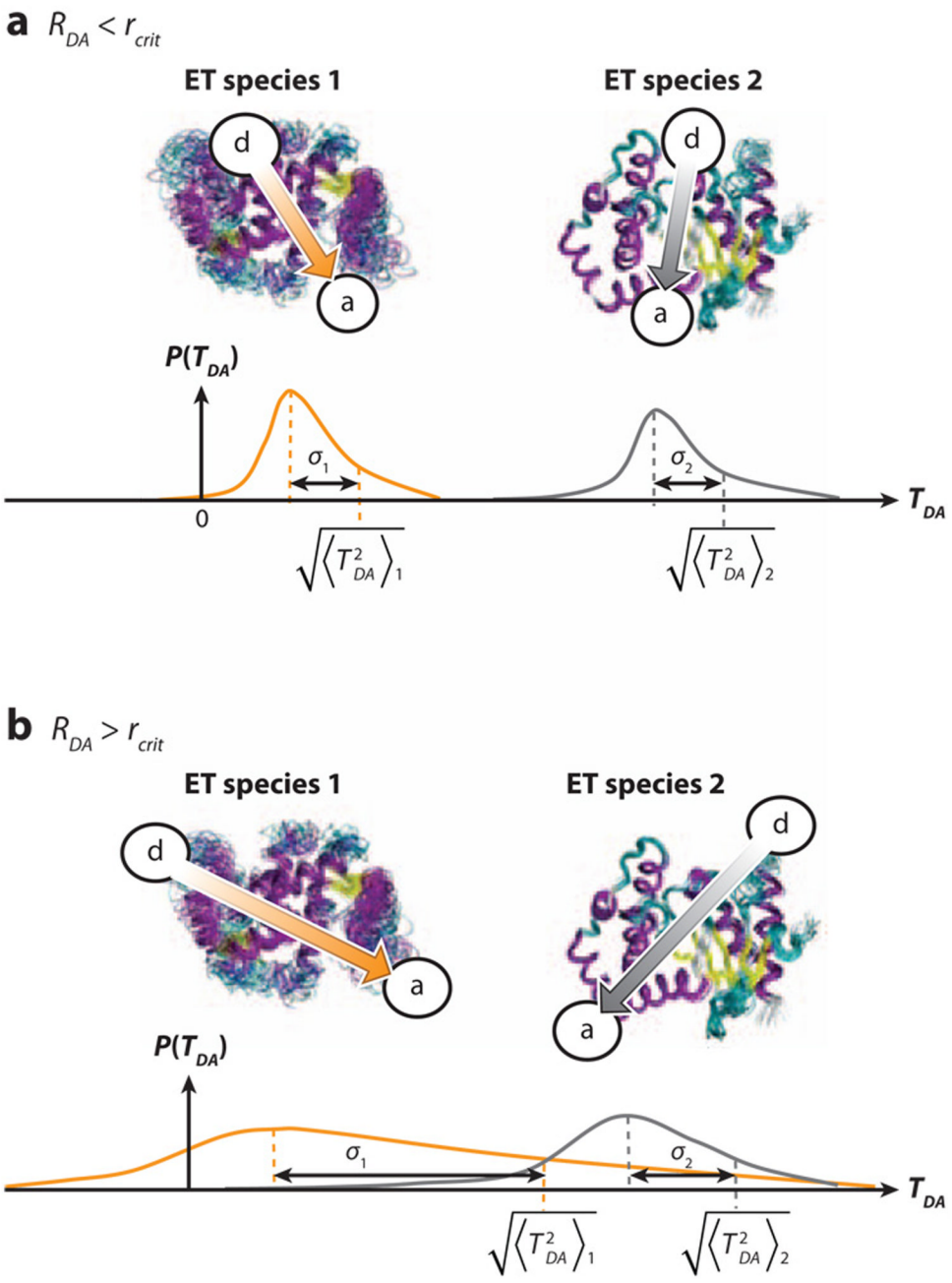

Figure 5.

Schematic diagram explaining how donor-acceptor (DA) coupling fluctuations could wash out DA coupling structural differences with increasing DA distance. The diagram shows possible T_{DA} probability densities for two pairs of different electron-transfer (ET) species, each pair having the same average values of R_{DA}. σ_1 and σ_2 represent the root-mean-squared coupling fluctuations $\sigma_{T_{DA}}$ of each species in the pair. (*a*) For $R_{DA} < r_{crit}$, coupling fluctuations are small and do not wash out structural differences in $\langle T_{DA}^2 \rangle$, i.e., $S_{R_{DA}<r_{crit}}=(\langle T_{DA}^2 \rangle_2 - \langle T_{DA}^2 \rangle_1)/(\langle T_{DA}^2 \rangle_2+\langle T_{DA}^2 \rangle_1)\sim 1$. (*b*) For $R_{DA} > r_{crit}$, the increase in coupling

fluctuations could wash out structural differences in $\langle T_{DA}^2 \rangle$, i.e., $S_{R_{DA}>r_{crit}} \ll 1$, leading to an average barrier limit. Surprisingly, our simulations do not observe this second regime (*b*) even though coupling fluctuations are large (45).

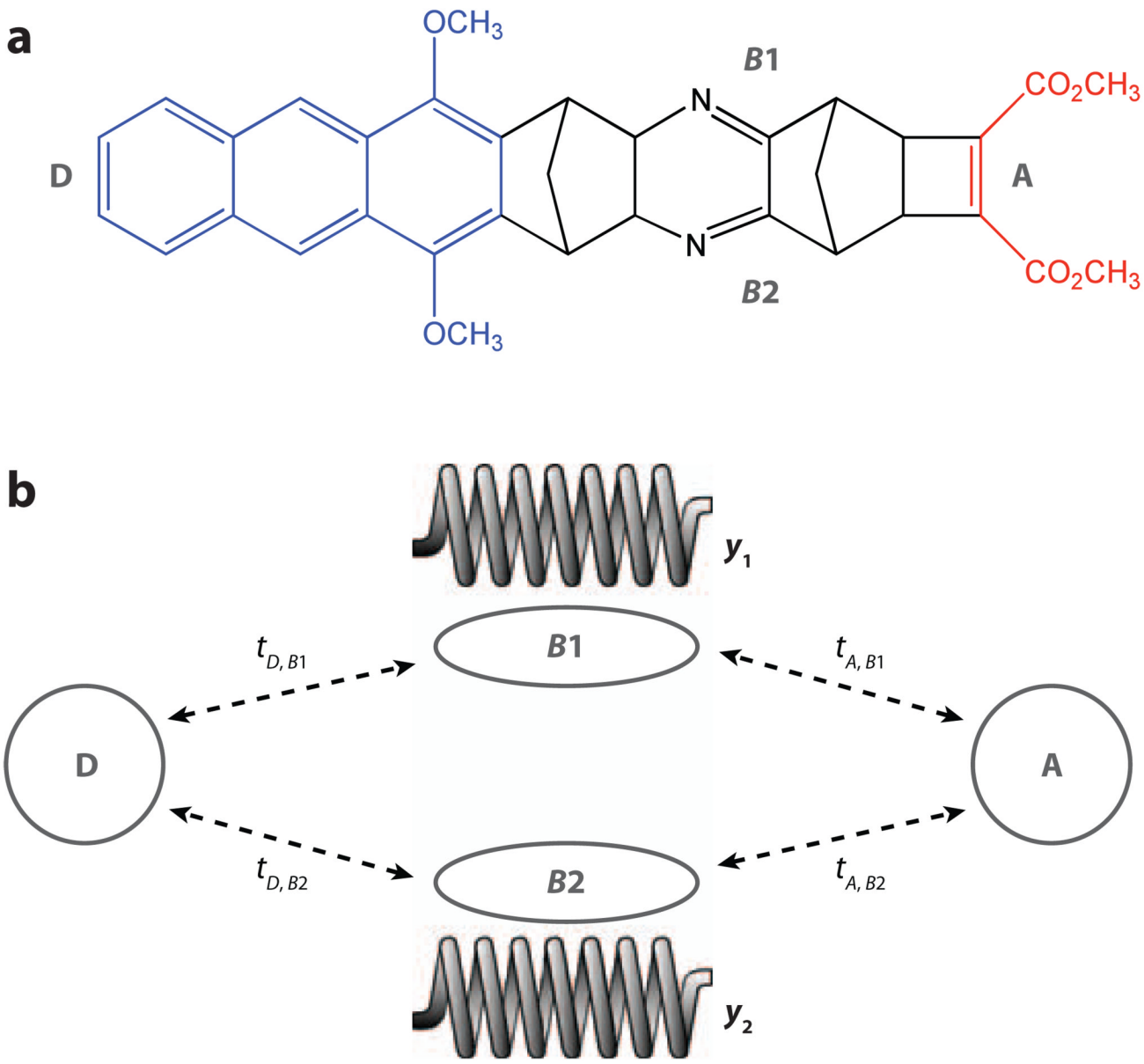

Figure 6.
(*a*) A donor-bridge-acceptor supermolecule that might be used to realize a molecular double-slit experiment. (*b*) The vibrations of the bridge could act to measure which pathway the electron follows as it tunnels from the donor (D) to the acceptor (A), if some of the atoms in one pathway are isotopically substituted in order to create pathway-localized vibrations.

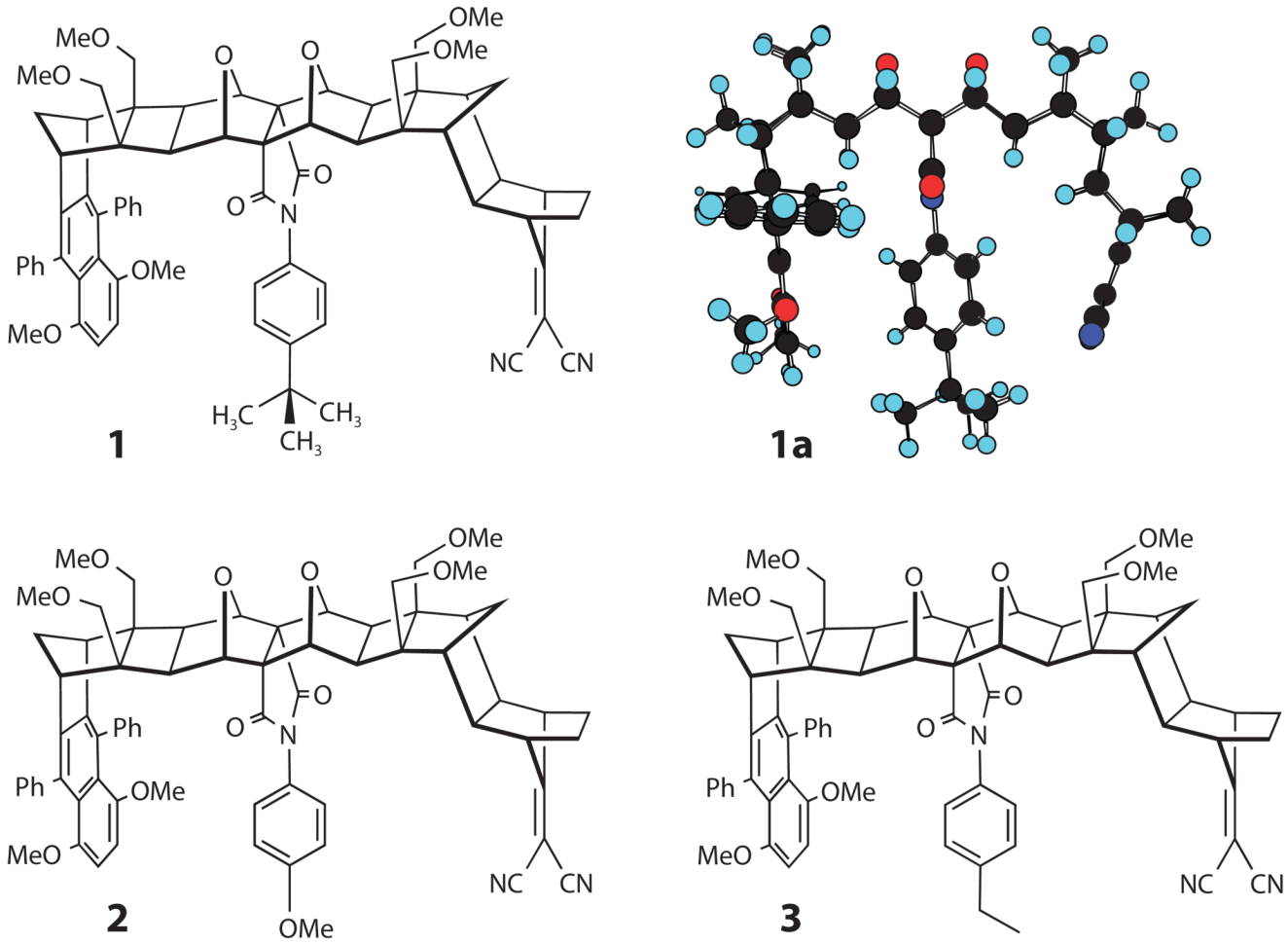

Figure 7.
Molecular structures for the three donor-bridge-acceptor supermolecules, which have different pendant groups in the line of sight between the naphthalenic donor and the dicyanoethylene acceptor units, that were studied by Paddon-Row, Waldeck, and coworkers.

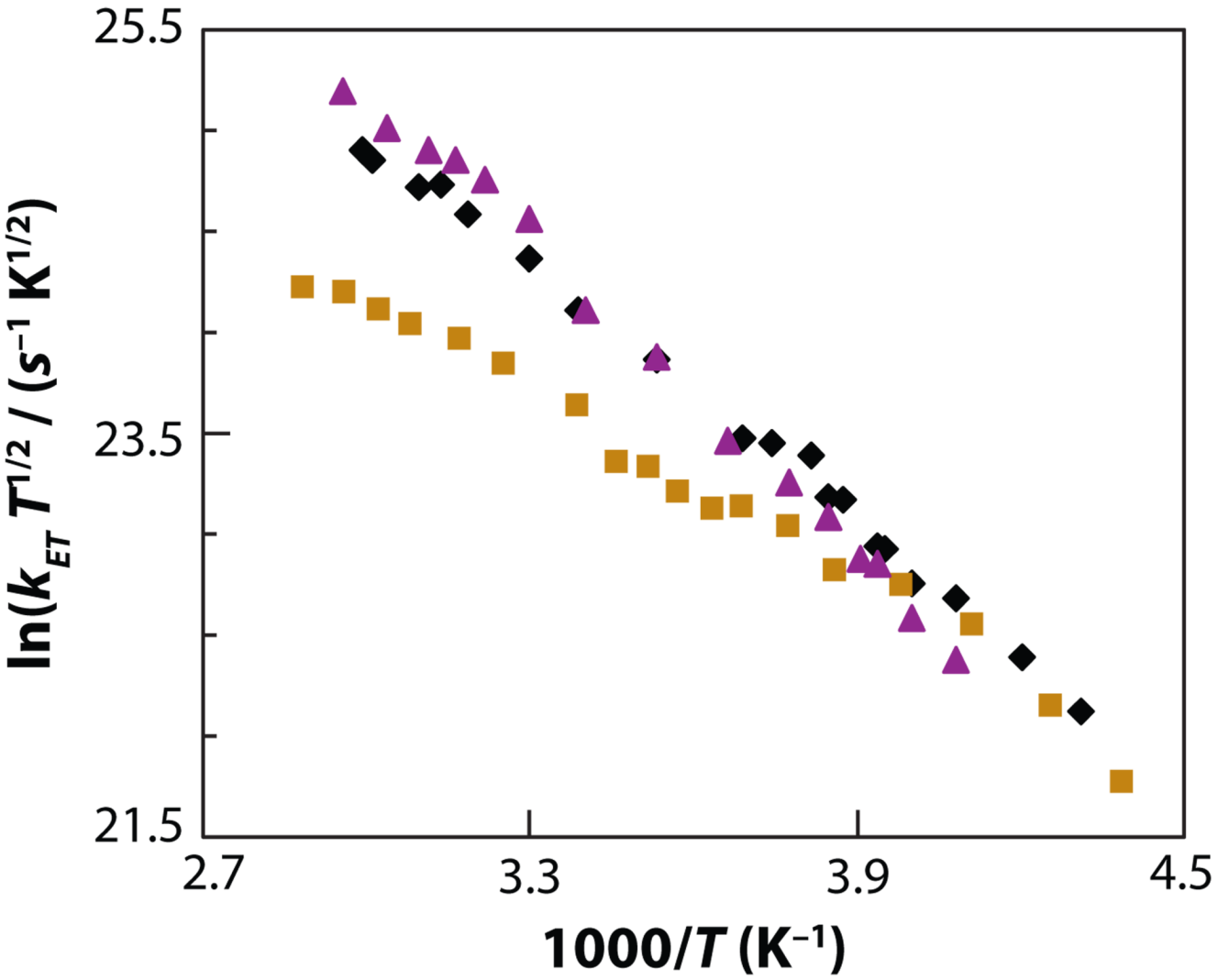

Figure 8.
Experimental electron transfer rate constants for compounds 1 (*gold squares*), 2 (*purple triangles*), and 3 (*black diamonds*) in NMP plotted versus the inverse of the temperature. Figure adapted with permission from Reference [93].

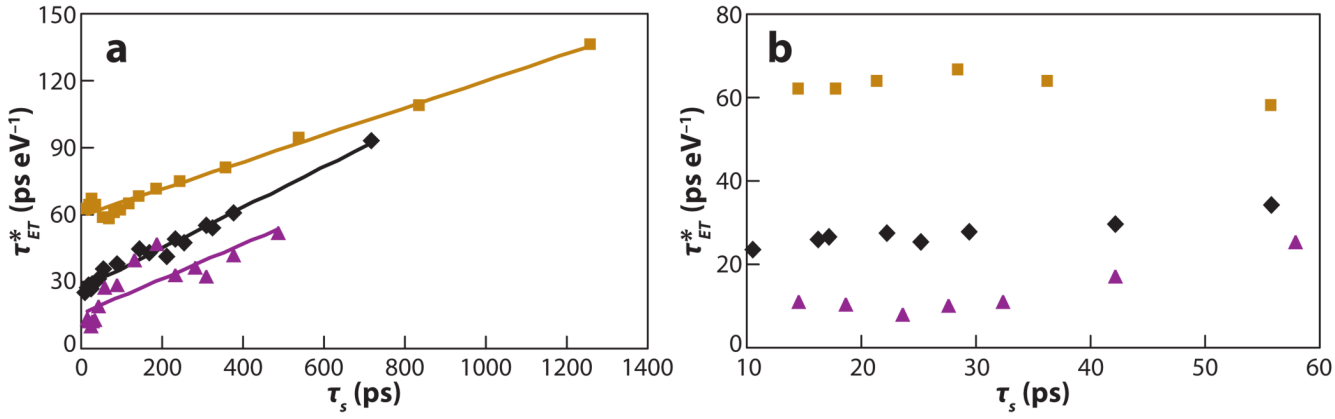

Figure 9.

Plot of τ^*_{ET} (Equation 25) versus τ_S for compound 1 (*gold squares*), compound 2 (*purple triangles*), and compound 3 (*black diamonds*) in NMP. (*a*) The plot over the whole range of data. (*b*) Expansion of the plot in the high-temperature region $0 \leq \tau_S \leq 60$ ps (60 ps corresponds to the room temperature) for compounds 1, 2, and 3. Figure adapted with permission from Reference [95].

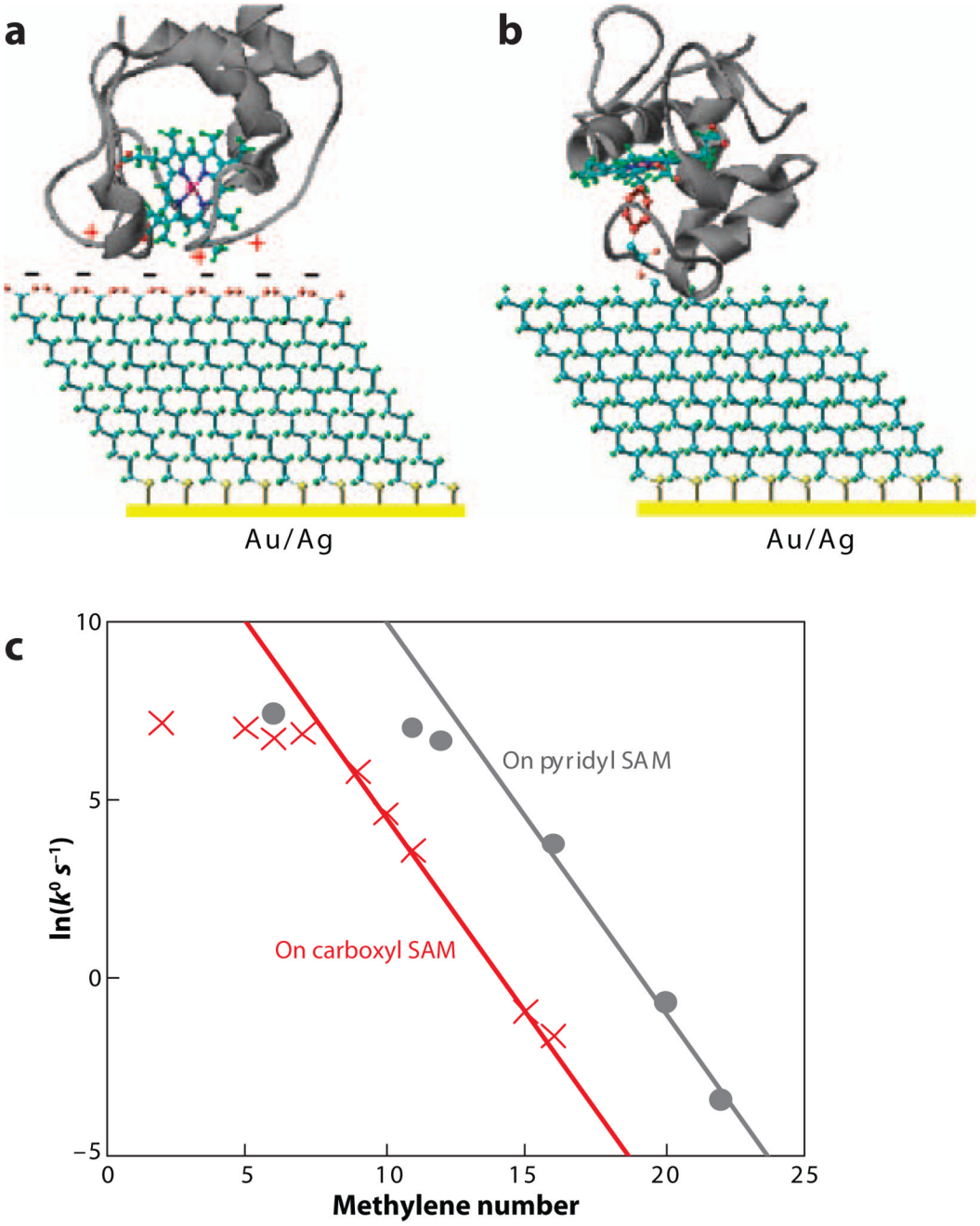

Figure 10.
Protein immobilized on self-assembled monolayer (SAM) surfaces: (*a*) Cytochrome *c* is absorbed electrostatically to a SAM of carboxylic acid terminated thiols, and (*b*) cytochrome *c* is tethered to a SAM by a pyridyl group that replaces Met 80 as an axial ligand. (*c*) Plots of ln(*k*°) versus the number of methylene groups in alkyl SAMs on Au.

Table 1

Fitting parameters for compound 1, 2, and 3 in N-methylpropionamide (NMP) at 295K[a]

Compound	$\|T_{DA}\|$ (cm^{-1})	λ (eV)	ΔG (eV)
1	90	1.24	−0.35
2	273	1.59	−0.57
3	147	1.50	−0.52

[a] See Reference 29.